

2

AD-A253 342



AEROSPACE REPORT NO.
TR-0089(4935-08)-1

An Investigation of the Effect of Low Velocity Impacts on P75/934 Graphite/Epoxy Composites

Prepared by

J. N. SCHURR, M. T. QUINN, and G. F. HAWKINS
Materials Sciences Laboratory
Laboratory Operations

1 April 1991

Prepared for

SPACE SYSTEMS DIVISION
AIR FORCE SYSTEMS COMMAND
Los Angeles Air Force Base
P. O. Box 92960
Los Angeles, CA 90009-2960

DTIC
ELECTE
JUL 28 1992
S. D.

Engineering and Technology Group

THE AEROSPACE CORPORATION
El Segundo, California

98 7 27 174

APPROVED FOR PUBLIC RELEASE;
DISTRIBUTION UNLIMITED

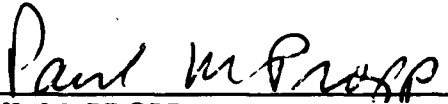
92-20257



This report was submitted by The Aerospace Corporation, El Segundo, CA 90245-4691, under Contract No. F04701-88-C-0089 with the Space Systems Division. P. O. Box 92960, Los Angeles, CA 90009-2960. It was reviewed and approved for The Aerospace Corporation by S. Feuerstein, Director, Materials Sciences Laboratory. Paul Propp was the project officer for the Mission-Oriented Investigation and Experimentation (MOIE) program.

This report has been reviewed by the Public Affairs Office (PAS) and is releasable to the National Technical Information Service (NTIS). At NTIS, it will be available to the general public, including foreign nationals.

This technical report has been reviewed and is approved for publication. Publication of this report does not constitute Air Force approval of the report's findings or conclusions. It is published only for the exchange and stimulation of ideas.



PAUL M. PROPP
Wright Lab West Coast Office
Materials Directorate



MARTIN K. WILLIAMS, Capt, USAF
Mgr, Space Systems Integration
DCS for Program Management

UNCLASSIFIED

SECURITY CLASSIFICATION OF THIS PAGE

REPORT DOCUMENTATION PAGE

1a. REPORT SECURITY CLASSIFICATION Unclassified			1b. RESTRICTIVE MARKINGS		
2a. SECURITY CLASSIFICATION AUTHORITY			3. DISTRIBUTION/AVAILABILITY OF REPORT Approved for public release; distribution unlimited		
2b. DECLASSIFICATION/DOWNGRADING SCHEDULE					
4. PERFORMING ORGANIZATION REPORT NUMBER(S) TR-0089(4935-08)-1			5. MONITORING ORGANIZATION REPORT NUMBER(S) SSD-TR-92-18		
6a. NAME OF PERFORMING ORGANIZATION The Aerospace Corporation Laboratory Operations		6b. OFFICE SYMBOL <i>(If applicable)</i>	7a. NAME OF MONITORING ORGANIZATION Space Systems Division		
6c. ADDRESS (City, State, and ZIP Code) El Segundo, CA 90245-4691			7b. ADDRESS (City, State, and ZIP Code) Los Angeles Air Force Base Los Angeles, CA 90009-2960		
8a. NAME OF FUNDING/SPONSORING ORGANIZATION		8b. OFFICE SYMBOL <i>(If applicable)</i>	9. PROCUREMENT INSTRUMENT IDENTIFICATION NUMBER F04701-88-C-0089		
8c. ADDRESS (City, State, and ZIP Code)			10. SOURCE OF FUNDING NUMBERS		
			PROGRAM ELEMENT NO.	PROJECT NO.	TASK NO.
			WORK UNIT ACCESSION NO.		
11. TITLE (Include Security Classification) An Investigation of the Effect of Low Velocity Impacts on P75/934 Graphite/Epoxy Composites					
12. PERSONAL AUTHOR(S) Schurr, Juliet N.; Quinn, Mary T.; and Hawkins, Gary F.					
13a. TYPE OF REPORT		13b. TIME COVERED FROM _____ TO _____		14. DATE OF REPORT (Year, Month, Day) 1 April 1991	
				15. PAGE COUNT 57	
16. SUPPLEMENTARY NOTATION					
17. COSATI CODES			18. SUBJECT TERMS (Continue on reverse if necessary and identify by block number)		
FIELD	GROUP	SUB-GROUP			
			Acoustic emission testing Laminate plates		
			Delamination Low velocity impact testing		
			Graphite/epoxy composites Mechanical strength testing		
19. ABSTRACT (Continue on reverse if necessary and identify by block number)					
<p>The low velocity impact testing of the P75/934 laminate plates revealed that this graphite/epoxy composite system is damaged very easily by impact. Impact energies to initiate damage as low as 6 ft-lb per inch thickness of composite were measured in drop-weight-type impact tests with edge supported, clamped specimens.</p> <p>Nondestructive evaluation (NDE) techniques, in particular, ultrasonic C-scan and dye enhanced X-ray radiography, confirmed that the damaged area increased with increased impact energy. The surface damage to the composite was detected visually only upon close inspection. Another promising NDE technique that was used to detect the presence of damage was thermal acoustic emission testing. Further study of this technique would be worthwhile pursuing.</p>					
20. DISTRIBUTION/AVAILABILITY OF ABSTRACT <input checked="" type="checkbox"/> UNCLASSIFIED/UNLIMITED <input type="checkbox"/> SAME AS RPT. <input type="checkbox"/> DTIC USERS				21. ABSTRACT SECURITY CLASSIFICATION Unclassified	
22a. NAME OF RESPONSIBLE INDIVIDUAL		22b. TELEPHONE (Include Area Code)		22c. OFFICE SYMBOL	

UNCLASSIFIED

18. SUBJECT TERMS (Continued)

Nondestructive evaluation	P75/934
Nondestructive testing	Residual strength
X-ray radiography	Ultrasonic testing

19. ABSTRACT (Continued)

Residual compression strength tests with a limited number of specimens showed that the specimens impacted with higher energies failed at lower stresses, as expected. Residual strength values of damaged laminates could not easily be compared to undamaged strength values because the specimens did not have the same laminate orientation as specified by the manufacturer. Discrepancies between the specified and actual laminate orientation were also uncovered in this investigation.

In addition, impact tests were performed on an HMS/934 Gr/Ep longeron part. For the longeron specimens, it was shown that internal damage may be induced even though no surface damage was visible after an impact occurred.

PREFACE

The authors wish to acknowledge the following people for their assistance in this program: R. Ruiz, ultrasonic C-scan; J. Hribar, acoustic emission; C. Su, specimen polishing and photography, and J. Doi, laminate orientation study. The helpful discussions with E. Y. Robinson are also greatly appreciated.

DTIC QUALITY INSPECTED 2

Accession For	
NTIS GRA&I	<input checked="checked" type="checkbox"/>
DTIC TAB	<input type="checkbox"/>
Unannounced	<input type="checkbox"/>
Justification	
By _____	
Distribution/	
Availability Codes	
Dist	Avail and/or Special
A-1	

CONTENTS

PREFACE.....	1
I. INTRODUCTION.....	9
II. OVERVIEW OF SAMPLES AND TESTS PERFORMED.....	11
III. LAMINATE ORIENTATION.....	13
A. NDT Specimens.....	13
B. CTE Specimens.....	16
C. LONG Specimens.....	18
IV. THERMAL ANALYSIS AND PHYSICAL PROPERTIES MEASUREMENT.....	21
V. MECHANICAL STRENGTH TESTING.....	23
VI. LOW VELOCITY IMPACT TESTING.....	27
A. NDT Specimens.....	27
B. LONG Specimens.....	31
VII. PRE- AND POST-IMPACT NONDESTRUCTIVE EVALUATION.....	35
A. X-Ray Radiography.....	35
B. Ultrasonics.....	36
C. Thermal-Acoustic Emission.....	45
D. Thermography.....	49
E. NDE Discussion.....	49
VIII. CROSS SECTIONING AND DEPLY ANALYSIS.....	51
IX. POST-IMPACT MECHANICAL TESTING.....	55
A. Compression Strength Testing.....	55
B. Acoustic Emission Monitoring During Compression Testing.....	56
X. CONCLUSIONS.....	61
REFERENCES.....	63

FIGURES

1.	Cross Section of Fibers Cut Along the 90° Normal.....	14
2.	Cross Section of Fibers Cut at an Angle, ϕ , from the 90° Normal.....	15
3.	Photomicrograph of CTE-6 Cross Sectioned at a Large Angle, ϕ , from the 90° Normal.....	17
4.	Photomicrograph of the Cross Section of LONG-1 Diagonal Longerons.....	19
5.	Average Tensile and Compression Strength Data for Various P75/934 Laminate Composites.....	25
6.	Calculated Longitudinal Tensile Modulus vs Laminate Orientation for Ultrahigh Modulus Type Composites.....	26
7.	Schematic of the Low Velocity, Drop-Weight Impact Testing Instrument.....	28
8.	Schematic of the Specimen Support Fixture for Impact Testing.....	28
9.	Plot of Load and Energy vs Time for NDT-4.11.....	30
10.	Schematic of the Diagonal Longerons.....	32
11.	X ray of Dye-Impregnated NDT-6.11, Highlighting Damaged Area.....	37
12.	Elliptical Damage Area Determined from X-ray Radiographs of Dye Enhanced Specimens and C-Scan Data vs Impact Energy for the NDT Specimens.....	38
13.	Elliptical Damage Area Determined from X-ray Radiographs of Dye Enhanced Specimens and C-Scan Data vs Impact Energy for the LONG Specimens.....	39
14.	C-Scan of Specimen NDT-6.11 Prior to Impact.....	41
15.	C-Scan of NDT-6.11 After Being Impacted with 15.6 in.-lb.....	41
16.	Detailed Scan of Damaged Area in NDT-6.11.....	43

FIGURES (continued)

17.	Thermal-Acoustic Equipment Setup Used to Monitor Acoustic Emission from the NDT Specimens.....	47
18.	Acoustic Emission from an Undamaged Specimen.....	48
19.	Acoustic Emission from Specimen NDT-4.11.....	48
20.	Photomicrograph of the Cross Section of NDT-6.11 After Impact.....	52
21.	Load History of NDT-4.11 During Acoustic Emission Monitoring.....	57
22.	Acoustic Emission of NDT-4.11 During Compression Loading.....	59

TABLES

1.	Test Performed on the NDT, CTE, and LONG Specimens.....	12
2.	Summary of Thermal Analyses and Physical Property Measurements.....	21
3.	Mechanical Strength Measurements of NDT-1, Ply Thickness, 0.003 in.....	23
4.	Impact Testing Results for the NDT Specimens.....	29
5.	Impact Testing Results for the LONG Specimens.....	33
6.	Compression Strength Testing Results for the NDT Specimens.....	55

I. INTRODUCTION

Graphite/epoxy composite materials are being used in the fabrication of large space structures. When using composite materials in this and other applications, there are concerns about the damage resistance of structures to inadvertent impacts during manufacturing and handling, the nondestructive detection of any internal damage generated, and the effect of impact damage on the load-carrying capability of the structure. The damage caused by low velocity impacts, such as delaminations, may not be apparent on the surface of a composite laminate. However, this damage can significantly reduce the composite's residual strength (Refs. 1-4). Detecting the damage and determining the effect of impacts to a particular composite system is thus a vital step in ensuring the performance of a composite structure.

In response to these concerns, we began investigating the sensitivity of P75/934 composite laminates, the material system used for a particular space program, to low velocity impact. This work includes determining the impact energy required to initiate damage in the laminate and examining the relationship between impact energy, damage area caused by impact, and residual compression strengths of the laminate. The issue of internal damage presence and damage severity without visual detectability is also addressed. Various destructive and nondestructive techniques are compared and used to evaluate the quality of the laminates. Verification of laminate orientation is also considered, since the composite laminate properties are directly related to the lay-up configuration. This characterization of the P75/934 system's response to impact will provide a guideline for protection and damage detection requirements of actual space structures. The drop-weight impact testing was geared toward producing nonvisible or barely visible damage. In addition, several flight hardware samples were checked for their ply lay-up and fiber orientation. Finally, several impact tests with pre- and post-impact nondestructive evaluation (NDE) were performed on an HMS/934 diagonal longeron section from the same space structure program.

II. OVERVIEW OF SAMPLES AND TESTS PERFORMED

Using a limited number of small test plates, material characterization, mechanical property testing, impact testing, destructive and nondestructive evaluation, and residual strength measurements were performed.

Three types of samples were studied: P75/934 laminate plates [referred to as the NDT (nondestructive testing) samples], P75/934 coefficient of thermal expansion coupons (the CTE samples), and an HMS/934 diagonal longeron (the LONG sample). The NDT samples--NDT-1, NDT-3, NDT-4, and NDT-6--were flat laminate plates manufactured specifically for non-destructive testing. Two of the four samples had small Teflon inserts between the center plies to simulate defects. From the four samples, (which were 16-, 16-, 48-, and 48-ply laminates, respectively), smaller specimens were sectioned, with either a diamond-edged blade or a carborundum blade, for the various tests. The CTE samples were actual flight hardware tag-end material used by the manufacturers for measurements. The LONG sample was a flight hardware component rejected because of incorrect dimensions. The CTE and LONG samples were also sectioned as necessary to produce various test specimens.

Table 1 presents an overview of the samples and tests performed. The laminate orientation of all samples was checked to see if the samples conformed to the specified fiber orientation and ply lay-up sequence. Thermal and physical properties were analyzed and mechanical strength was tested to further characterize the composite material. The resistance of materials to impact damage was determined from the low velocity impact testing. The damage caused by impact was examined using various nondestructive and destructive techniques. Finally, post-impact mechanical testing was performed to investigate the effect of impact damage on the strength of the material.

Table 1. Test Performed on the NDT, CTE, and LONG Specimens

Sample	Description	Gr/Ep	Laminate Orientation	Thermal and Physical Properties Analysis	Mechanical Strength Testing	Impact Testing	Pre- and Post-Impact NDE	Post-Impact Cross-Section and Deploy	Post-Impact Mechanical Testing
NDT	(4) 9"x9" Plates	P75/934	X	X	X	X	X	X	X
CTE	(3) 1"x7 7/8" coupons	P75/934	X						
LONG	(1) 35 1/2"x3 1/4" hat-shaped longeron	HMS/934	X			X	X		

III. LAMINATE ORIENTATION

The fiber orientation and ply lay-up sequence of the laminates were checked by cutting and polishing the specimens along the 0° direction and observing the cross-sectional shape of the fibers. When a specimen is cut along the 90° normal, as shown in Fig. 1, then the fibers aligned in the 0° direction appear as lines, the 90° fibers as circles, and all other angle fibers as ellipses with an aspect ratio of $2a/2b$. With this plane of polishing, the ellipses appear the same for a positive angle as for the corresponding negative angle. When the specimen is cut at an angle, θ , from the 90° normal, as shown in Fig. 2, all fiber directions can be distinguished.

A. NDT SPECIMENS

NDT-1 and NDT-3 were specified by the manufacturer to be $[0/+52/-52/90]_{2s}$ laminates, whereas NDT-4 and NDT-6 were specified to be $[0/+52/-52/90]_{6s}$ laminates. According to standard code interpretation (Ref. 5), $[0/+52/-52/90]_{2s}$ signifies a 16-ply laminate, where the first 4 plies have fibers oriented in the $0, +52, -52$, and 90° directions. The next 4 plies repeat that sequence, and the following 8 plies are in the reverse order, so that they are symmetric with the first 8 plies. The laminate $[0/+52/-52/90]_{6s}$ is a 48-ply laminate, where the $0, +52, -52, 90$ sequence is repeated 6 times, followed by 24 plies symmetric to the first 24 plies. The first ply is the first to be laid on the tool surface. Thus, this outer ply has a smooth surface, as opposed to the last ply, which is on the vacuum bag side and acquires the rough texture of the resin bleeder cloth. Fiber angles increase in a counterclockwise direction when viewed toward the bag side of the laminate. Conversely, when viewed toward the tool side of the laminate, positive angles are clockwise to the 0° direction.

The laminate orientation results for specimens NDT-1 and NDT-4 were previously analyzed, and it was determined for NDT-1 that all but

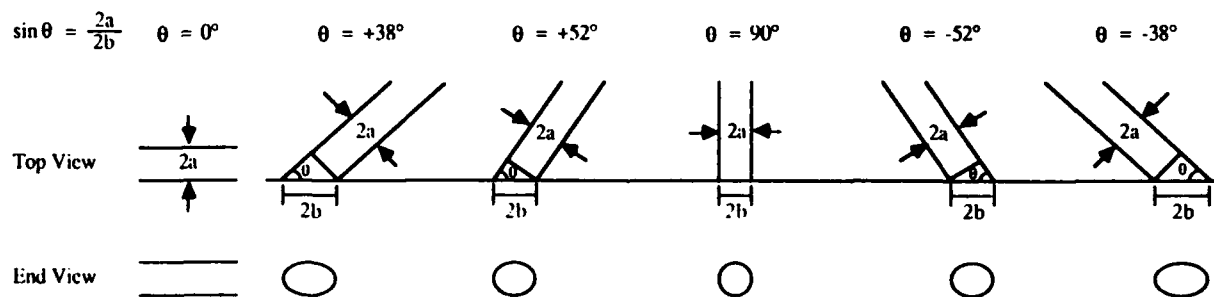
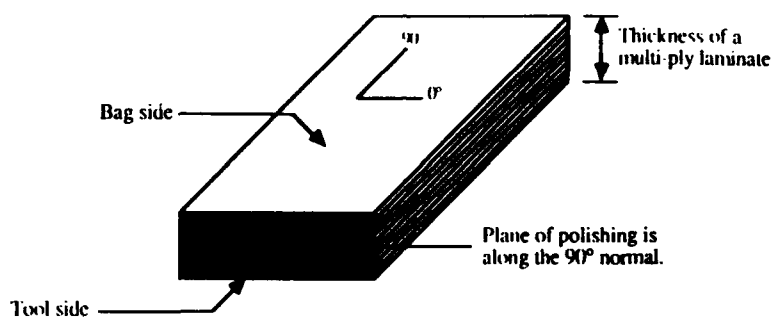
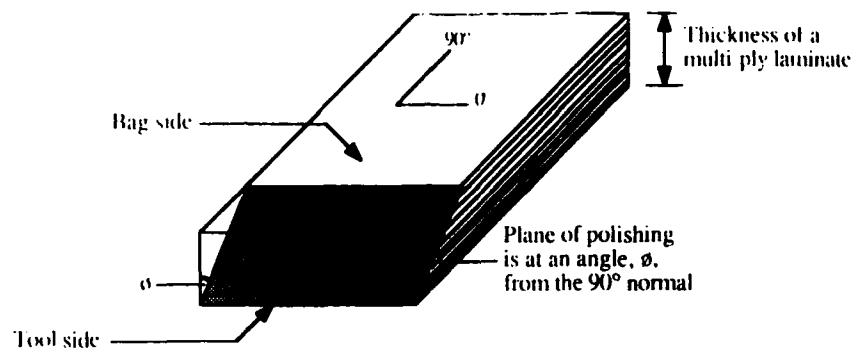


Fig. 1. Cross Section of Fibers Cut Along the 90° Normal



For $\phi = 45^\circ$, $\sin \theta = \sqrt{2} \left(\frac{2a}{2b} \right)$ where $2a$ and $2b$ are the lengths of the minor and major axes respectively

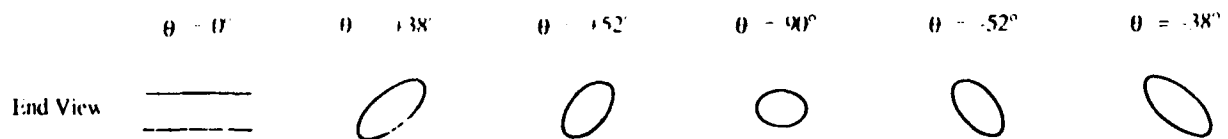


Fig. 2. Cross Section of Fibers Cut at an Angle, ϕ , from the 90° Normal

one of the 52° angled plies were erroneously laid up at 38°. In addition, the plane of symmetry occurred after the fourth ply, and the following 8 plies exactly repeated the first 8 plies. NDT-4 was similar, except that almost as many plies had fibers that were oriented closer to 38° than to 52°. Thus, not only were there incorrect fiber orientations, the lay-up sequence did not conform to the laminate code specified. With the cross sectioning performed on these plies, positive angles could not be distinguished from negative angles.

NDT-3 and NDT-6 were cross sectioned and polished at a 45° angle from the 90° normal. In NDT-6, several plies that should have had 52° fibers instead had fibers closer to 38°. Like NDT-1 and NDT-4, NDT-3 and NDT-6 had lay-up sequences where the planes of symmetry occurred after each 0,+52,-52,90 sequence instead of only once at the center of the laminate. In other words, instead of $[(0/+52/-52/90)_n]_s$, where $n = 2$ or 6 , the laminates were $[(0/+52/-52/90)_s]_n$, disregarding some of the 52° fibers that were replaced with fibers closer to 38° in NDT-6.

B. CTE SPECIMENS

The CTE specimens were sectioned and polished at an angle like the NDT specimens. However, the polishing was done at a very large angle from the 90° normal. Figure 3 exhibits the photomicrograph of the resulting cross section for CTE-6, viewed from the tool side of the laminate. CTE-2, CTE-6, and CTE-9 were specified by the manufacturer to be $[+46/-46/0/90/90/0/-46/+46]_n$, where $n = 4, 2$, and 3 , respectively. All CTE specimens had the specified lay-up sequence and fiber orientation.

To analyze the fiber orientation and ply lay-up sequence of a laminate, a clear description of the laminate should first be given. If the standard laminate code notation is not used, the laminate should be specified simply and unambiguously. Then, when the laminate is checked for conformance to the specified lay-up, a reasonable assessment can be made.

Note that all fiber angles reported in this work are approximate. When a laminate is sectioned at a large angle from the 90° normal, all fiber angles are quickly revealed and can be roughly determined by

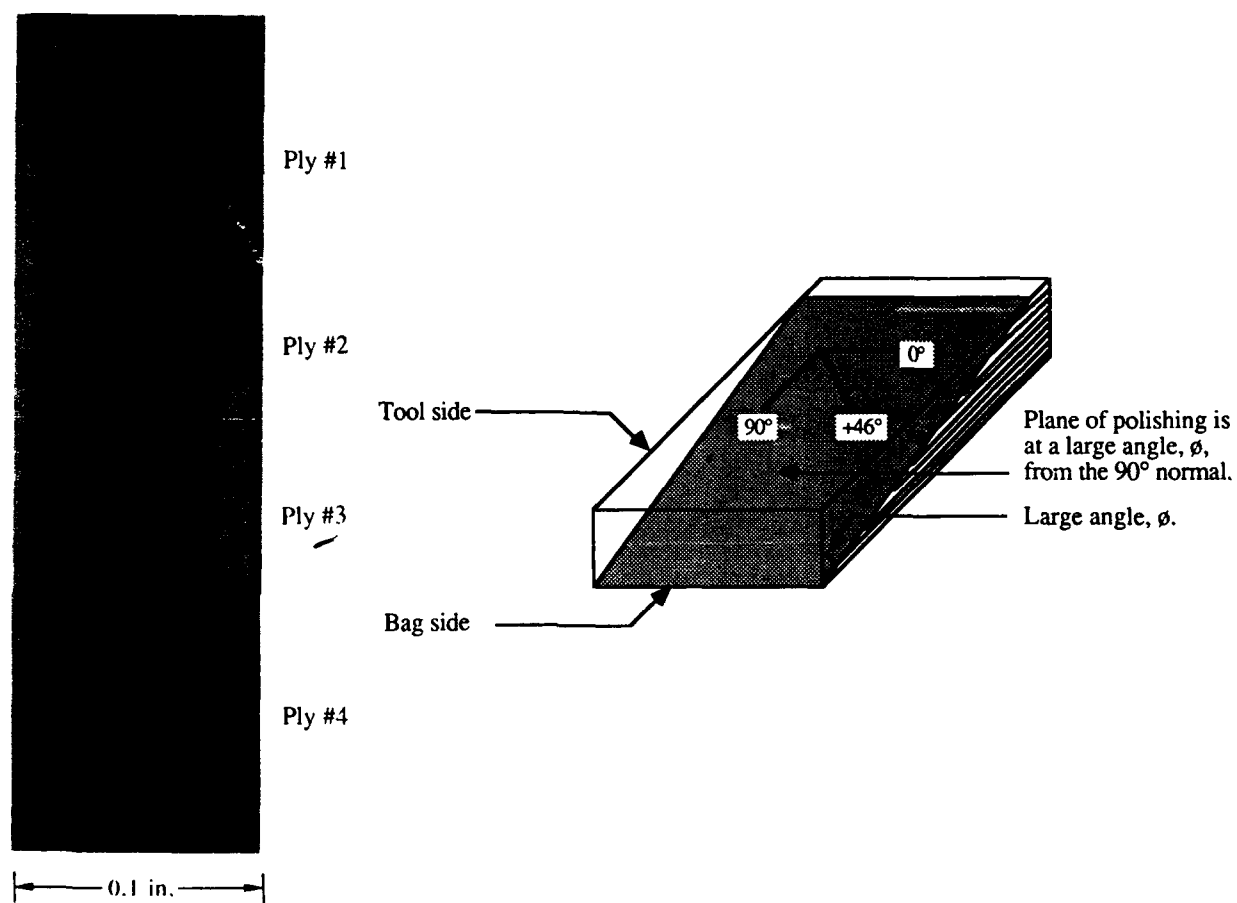


Fig. 3. Photomicrograph of CTE-6 Cross Sectioned at a Large Angle, ϕ , from the 90° Normal

measuring the angle between the fibers. For CTE-6, Fig. 3 indicates that fibers within the same ply (see ply No. 1, for example) may be several degrees off the intended angle. When a laminate is sectioned at some smaller angle, such as $\phi = 45^\circ$, from the normal, it has been observed that the elliptical cross sections are not uniform. This also suggests that the fibers do not have exactly the same orientation. Thus, fiber orientations appear to vary, even within the same ply. In an in-depth study, the elliptical shapes of many fibers could be analyzed, and each ply could be more accurately described with a statistical distribution of fiber orientations. A digital image analyzer would be required to perform this tedious task. For the NDT specimens, the elliptical cross sections were visually examined to identify whether the fibers were oriented closer to 52° or 38° direction; the cross sections were not examined for an exact angle determination. Likewise, the CTE laminate orientations were checked for their general agreement with the specified lay-up.

C. LONG SPECIMENS

The diagonal longeron component lay-up was specified by the manufacturer to be $[0/+39/90/-39/0]_3s$. The hat-shaped diagonal longeron is an HMS/934 composite with a specified "cap" thickness of 0.21 in. and a thickness of 0.09 in. in the web and flange (see Fig. 4). A cross-sectional examination of LONG-1, a specimen cut off the end of the diagonal longeron, indicated that the cap area was composed of 70 plies. The laminate orientation was $[(0/-x/90/+x/0)s]_7$. The angle, x , was not measured for all plies but was shown to vary between 45° and 55° for the first four plies. All positive angles appeared to be replaced with negative angles, and vice versa.

The number of plies decreased from 70 to 30 from the cap area to the web and flange of the hat shaped longeron. Plies Nos. 11-29 and Nos. 41-59 gradually dropped off, leaving 30 plies. At both ends of the diagonal longeron, there was an extra cloth-weave-type layer over the 70 plies, which extended about 4 in. across the cap. Several wrinkles were observed on the bag side surface, where the web and flange of the diagonal longeron meet.

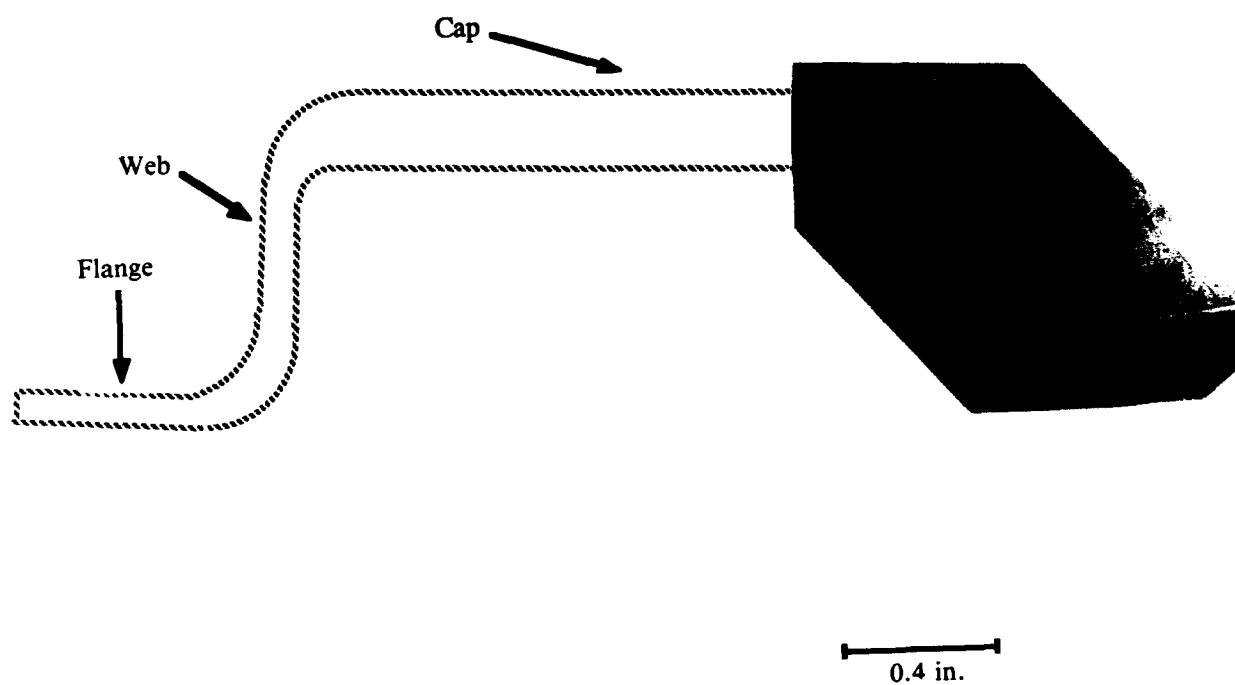


Fig. 4. Photomicrograph of the Cross Section of LONG-1 Diagonal Longeron

IV. THERMAL ANALYSIS AND PHYSICAL PROPERTIES MEASUREMENT

One differential scanning calorimetry (DSC) run and one thermogravimetric analysis (TGA) run were performed on NDT-1, NDT-4, and NDT-6. All three NDT plates had similar DSC and TGA curves. The graphical results are summarized in Table 2. More precise T_g values will require further DSC testing, as the T_g values were difficult to determine from these curves. The first exotherm at 220° C corresponds to further cross-linking in the resin. This correspondence indicates that the maximum temperature to which these samples were exposed during cure must have been less than 220°C. The second exotherm near 375°C indicates a decomposition process. This process is validated by the TGA results, which indicate that significant weight loss occurs between 300 and 500°C.

The fiber weight percent of the laminates was determined using the ASTM D3171-76, entitled Standard Test Method for Fiber Content of Resin-Matrix Composites by Matrix Digestion. Laminate densities were determined using a methanol immersion density technique. These results are also shown in Table 2.

Table 2. Summary of Thermal Analyses and Physical Property Measurements

Specimen	DSC	TGA	Wt.% Fiber	Density (g/cm ³)
NDT-1	Tg~60°C, Small Exotherms at 220, 380°C	Wt.Loss Begins ~300°C continues to 500°C	72.5	1.76
NDT-4	Tg~55°C, Small Exotherms at 220, 370°C	Wt.Loss Begins ~300°C continues to 500°C	72.4	1.77
NDT-6	Tg~55°C, Small Exotherms at 220, 375°C	Wt.Loss Begins ~300°C continues to 500°C	75.1	1.77

V. MECHANICAL STRENGTH TESTING

Standard compression strength tests for graphite/epoxy composites were conducted using Boeing Material Specification BMS 8-212E. The 3.18 x 0.50 in. coupon samples with 1.50 in. length fiberglass/epoxy end tabs were compressed to failure at a test rate of 0.05 in./min. Tensile strength and modulus were measured according to the procedures in ASTM D 3039-76(82). The 9.00 x 0.50 in. coupons with 2.00 in. length fiberglass/epoxy end tabs were loaded to failure at a rate of 0.05 in./min. Five specimens were each tested for compression and tensile strength. Tensile modulus, Poisson's ratio, and strain to failure values were determined from the tensile tests. All specimens were taken from the 16 ply NDT-1 plate and were loaded along the 0° fiber direction. The results shown in Table 3 are the average values from five tests. Delsen Testing Laboratories, Glendale, California, performed all specimen preparation and mechanical testing.

Table 3. Mechanical Strength Measurements of NDT-1,
Ply Thickness, 0.003 in.

Compression Strength (ksi)	36
Tensile Strength (ksi)	46
Tensile Modulus (msi)	16
Poisson's Ratio	0.42
Strain to Failure	0.30%

Some mechanical strength values provided by the composite manufacturer were 27.3 and 24.0 ksi, for the tensile and compression strength, respectively. These strength measurements are for four types of laminates P75S/934 [(±46/0/90)s]2,3,4,6, tested by the manufacturer in the 0° direction. The test values may be low because of samples breaking at the loading grips and not in the center. In contrast, the NDT-1 specimens

tested at Delsen Laboratories appear to have failed near the center of the specimen; the test values, 45 and 36 ksi, should therefore be a fair indication of actual tensile and compression strengths for these laminates. Note, however, that NDT-1 essentially had a $[(0/+38/-38/90)_s]_2$ lay-up, except that one of the 38° plies was replaced with a 52° ply.

Other researchers (Ref. 6) measured average ultimate tension and compression strength values of 39.5 and 26.4 ksi, respectively, for a $[(0/+45/-45/90)_s]_n$ P75S/934 laminate. These strength values are lower than those of NDT-1, as would be expected of a laminate with fibers oriented further from the 0° test axis. Figure 5 is a plot of all available mechanical strength data for the various P75/934 laminate orientations.

The effect of ply lay-up on the variation of longitudinal tensile modulus, E_x , is illustrated in Fig. 6 for several laminate orientations. The moduli were computed assuming the following monoply properties: longitudinal modulus, $E_x = 42$ ksi; transverse modulus, $E_y = 1.5$ ksi; shear modulus, $G_{xy} = 0.5$ ksi; and Poisson's ratio, $\nu = 0.3$ (typical values for ultrahigh modulus graphite/epoxy unidirectional prepreg tape). The longitudinal modulus increases as the $\pm \theta$ angle fibers approach the 0° direction, i.e., $[(0/\pm 38/90)_s]_n$ has a higher modulus than $[0/\pm 45/90)_s]_n$, which has a higher modulus than $[(0/\pm 46/90)_s]_n$. In addition, when one 38° ply is replaced with a 52° ply in $[0/\pm 38/90)_s]_2$, as in the case of NDT-1, the tensile modulus is lowered. The NDT-1 specimen modulus value, also included in Fig. 6, was found to be less than the computed value. Actual monoply moduli and Poisson's ratio values may not have matched those assumed in the computed laminate modulus.

Strength and modulus values of a composite laminate are dependent on the laminate orientation. Thus, in order to predict a composite laminate's performance, an accurate characterization of a laminate's orientation is required.

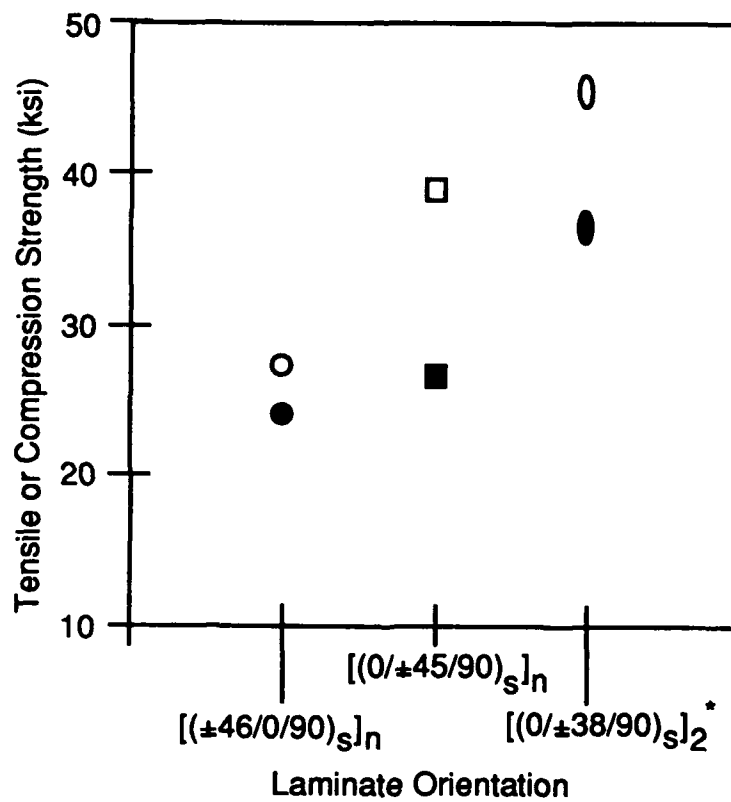


Fig. 5. Average Tensile (open symbols) and Compression (filled symbols) Strength Data for Various P75/934 Laminate Composites.

Circles - composite manufacturer; Squares - Johnson, Cushman; Ovals - our data.

*Note: One of the 38° plies was replaced with a 52° ply.

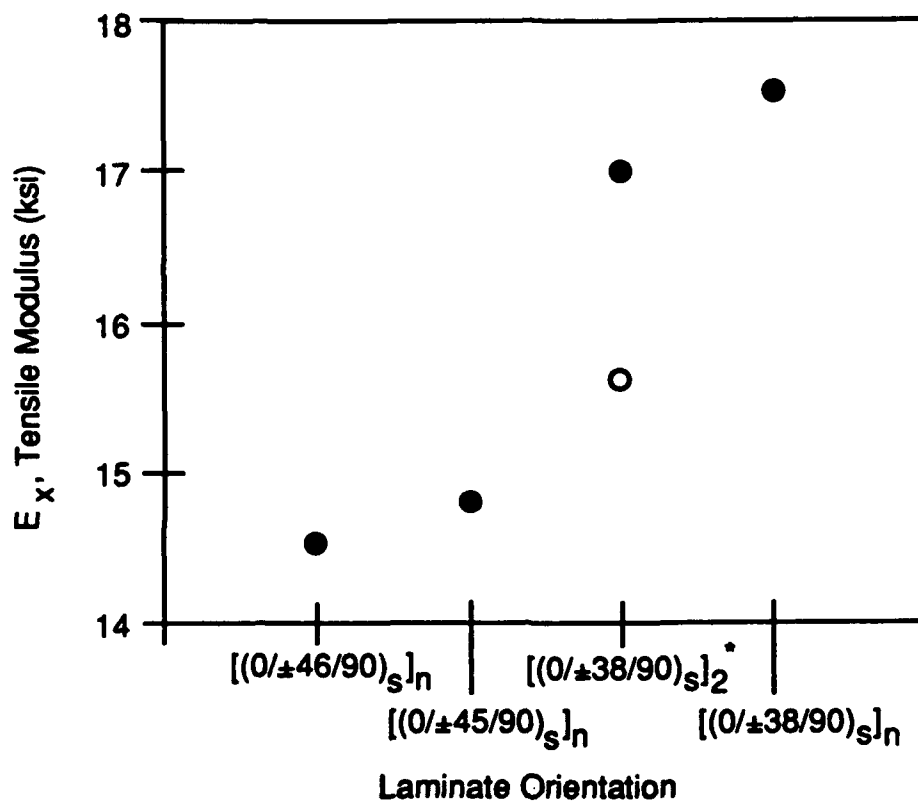


Fig. 6. Calculated Longitudinal Tensile Modulus (filled circles) vs Laminate Orientation for Ultrahigh Modulus Type Composites. Measured longitudinal tensile modulus (open circle) for the P75/934 NDT-1 specimen.

*Note: One of the 38° plies was replaced with a 52° ply.

VI. LOW VELOCITY IMPACT TESTING

The low velocity impact testing was performed using an instrumented drop-weight system. Figure 7 is a schematic of this system, which uses the Dynatup drop tower with associated instrumentation. A 5/8 in. spherical tip steel impactor attached to the crosshead impacted the sample from various heights. By changing the drop height, the impact velocity and thus the energy of impact could be varied. The load as a function of time was measured by the load cell attached to the impactor. The impact velocity was determined from the interruption time of a flag attached to the falling crosshead passing through an infrared (IR) beam. Once the impactor hit the specimen, the crosshead was stopped on the rebound to prevent multiple impacts.

A. NDT SPECIMENS

The NDT impact specimens were cut into 4.0 x 6.0 in. plates in accordance with Boeing Specification Support Standard BSS 7260, entitled Advanced Composite Compression Tests: Plate Compression After Impact Test (1983). Figure 8 shows how the plate is positioned over a 3 x 5 in. window and clamped into place. Five NDT specimens were impact tested; all were impacted on the bag side of the laminate. Four of the five specimens were 48-ply laminates; the fifth specimen, NDT-3.10, was a 16-ply laminate. The results of the impact tests are listed in Table 4.

From various experimental impact work in the literature (Refs. 2,4, 8-14), it was estimated that between 60 and 90 in.-lb of impact energy would cause some visible surface damage to the specimens. However, as the test results show, a 73.3 in.-lb impact caused the impactor to completely penetrate the first specimen, NDT-4.10. Delsen Testing Laboratories, where NDT-4.10 was tested, could not provide a lower energy of impact, so the remaining specimens were tested at General Research Corporation (GRC), Santa Barbara, California. GRC used a crosshead weight of 5.39 lb, which could be released from drop heights as low as 1 in.

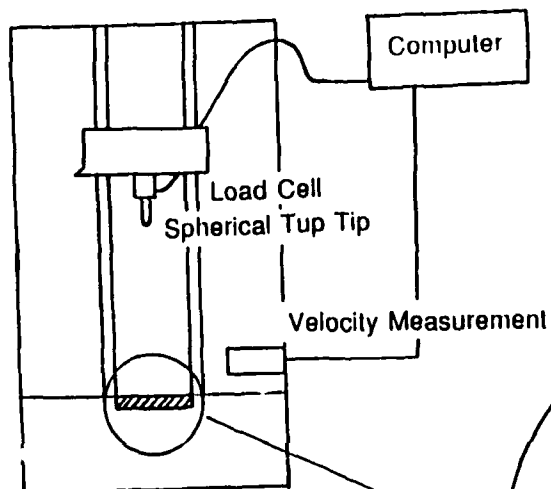


Fig. 7. Schematic of the Low Velocity, Drop-Weight Impact Testing Instrument

Drop Weight, $m_d = 11.39$ or ± 39 lb

Drop Height, $h = \text{adjustable}$

Tup Velocity, $v = \sqrt{v_0^2 + 2gh}$

Tup Energy, $E = 1/2 mv^2$

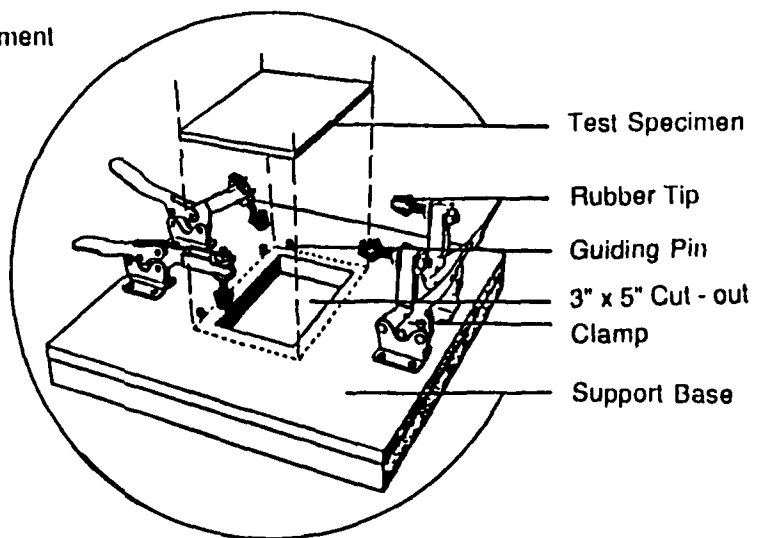


Fig. 8. Schematic of the Specimen Support Fixture for Impact Testing

Table 4. Impact Testing Results for the NDT Specimens

Specimen	Laminate Thickness (in.)	Impact Energy (in.-lb.)	Visible Damage		Incipient Energy (in.-lb.)	Incipient Energy per Thickness (ft.-lb./in.)
			front	back		
NDT-4.10	0.14	73.3	hole	hole, large bulge detached plies	6.4	3.8
NDT-4.11	0.14	24.0	slight indentation	cracks slight bulge	10.4	6.2
NDT-6.10	0.13	10.7	none	cracks	9.8	6.3
NDT-6.11	0.13	15.6	none	cracks	9.6	6.2
NDT-3.10	0.055	5.3	none	cracks	1.3	2.0

As the results show, an impact energy of 24.0 in.-lb produced visible damage to the front and back surfaces of the specimens, whereas energies less than 24.0 in.-lb only produced cracks on the back surface. Note that even with the lowest impact energy, there was always some visible damage.

The measured load and calculated absorbed energy vs time plot for NDT-4.11 is shown in Fig. 9. When the impactor first hits the specimen, the load rises linearly as the specimen undergoes elastic deformation. Then there may be yield behavior with increased damage to the impacted plate. The load continues to rise to a maximum, at which point the load drops suddenly, indicating brittle failure.

The energy corresponding to the point at which the load curve first dips or changes slope (incipient load) is normally referred to as the incipient energy (Ref. 15). The incipient energy value measures the absorbed energy required to initiate damage, as indicated on the load curve by the

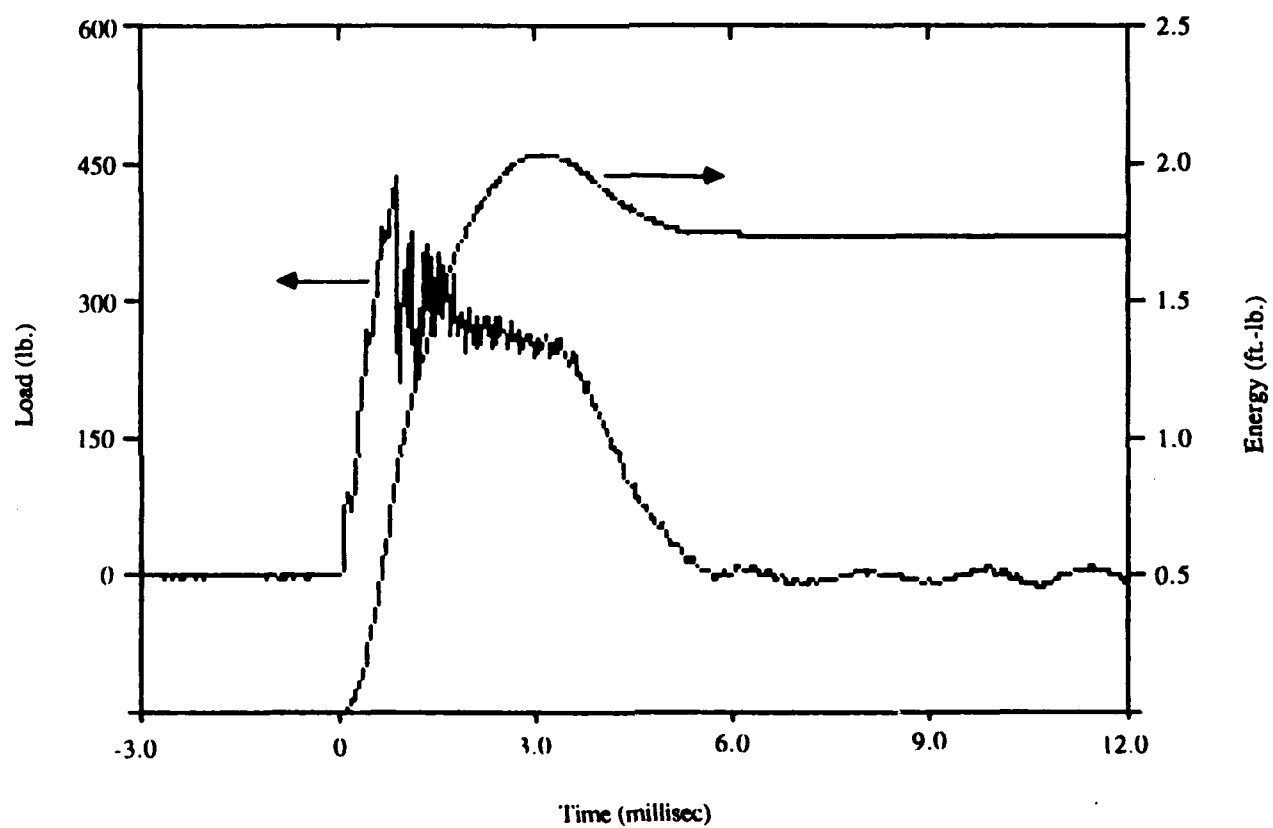


Fig. 9. Plot of Load and Energy vs Time for NDT-4.11

reduction in specimen stiffness. The incipient load is not always obvious on the load curves. The load signal may have extraneous fluctuations because of the dynamic interactions between the specimen and the impactor, or the change in slope may be very subtle. To simplify matters, for NDT-4.10, -4.11, -6.10, and -6.11, we considered the incipient load to be the same as the maximum load. Table 4 reveals that for three of the four samples of comparable thickness, the incipient energy was approximately 10 in.-lb. NDT-4.10, the through-penetration specimen, had a lower value of about 6 in.-lb.

If one considers the incipient energy per thickness of sample, all five specimens measure approximately 6 ft-lb/in. or less. According to some previous GRC testing of various graphite/epoxy laminates (with a thickness comparable to the 0.14 in. specimens, tested by the same BSS 7260 procedure), it was found that 25-50 ft-lb/in. was typical for the incipient-energy-per-thickness measurement.* In comparison, then, these P75/934 laminates are more sensitive to the initiation of damage by impact than other graphite/epoxy systems. NDE of the damaged area and residual strength measurements are presented later in this report and reveal the extent of damage and the effect of the impact on the sample strength.

B. LONG SPECIMENS

The hat-shaped diagonal longeron was cut into three sections: 12, 12, and 11 in. long. Each section was impacted in two locations on the top of the cap area, as shown in Fig. 10. The longeron sections were clamped along the flange in a support fixture slightly different from the one used for the NDT plates. Instead of centering the specimen over a 3 x 5 in. window, the longeron was placed over a 2 9/16 in. circular opening for each impact location. Because of the slight twist in the diagonal longeron, steel shims had to be placed under the longeron at the clamps, so that the part would lay flat on the support fixture. The results of the impact test are listed in Table 5.

*Discussion with Dr. M. Hahn, GRC, September 1988.

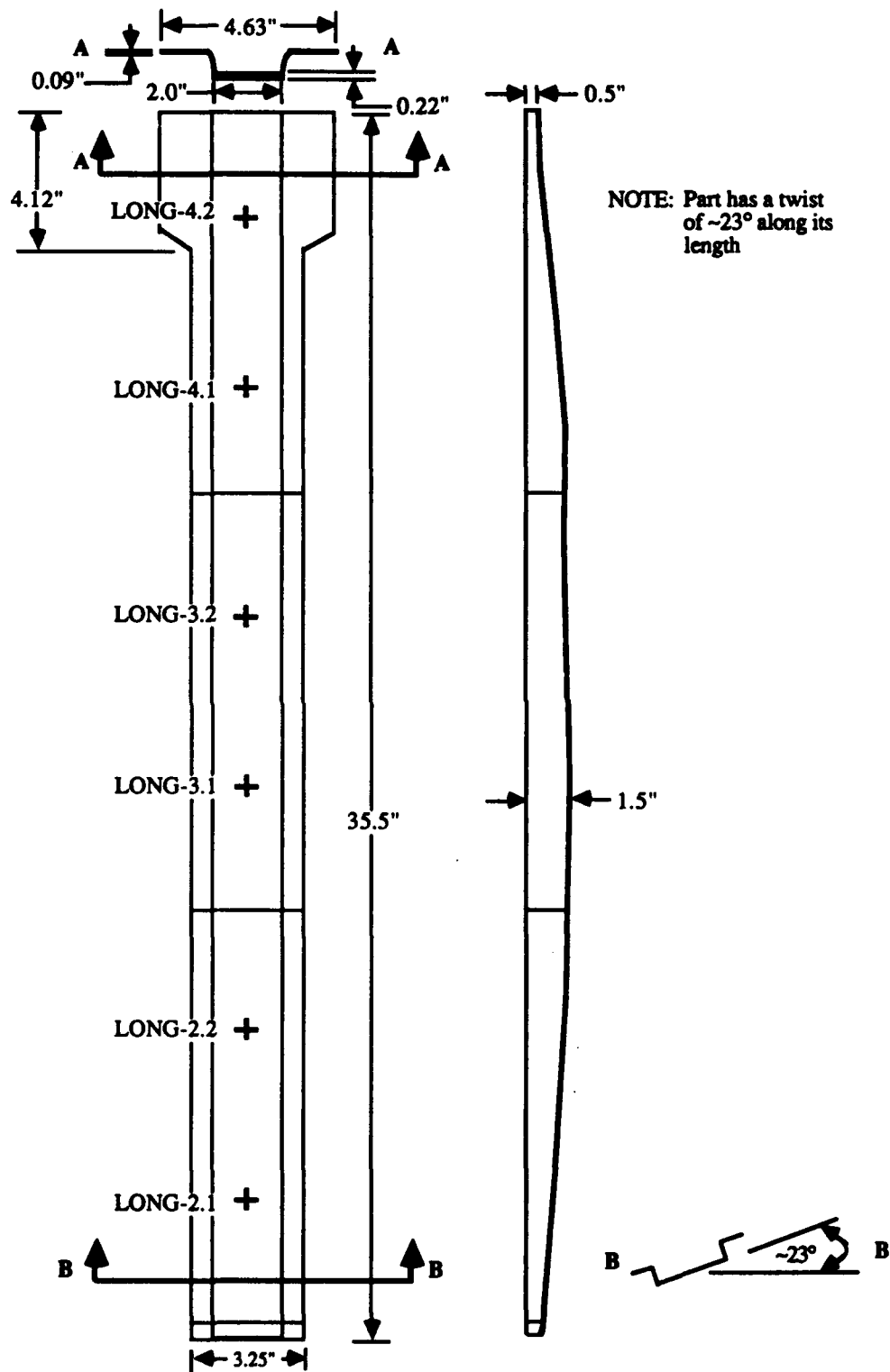


Fig. 10. Schematic of the Diagonal Longerons

Table 5. Impact Testing Results for the LONG Specimens

Specimen	Impact Energy (in.-lb.).	Visible Damage		Incipient Energy (in.-lb.)
		front	back	
LONG-2.1	108, 27 ^a	slight indentation	crack	10.4
LONG-2.2	54.7	none	none	11.3
LONG-3.1	162	large indentation	cracks large bulge	12.0
LONG-3.2	80.5	none	none	5.8
LONG-4.1	82.4	none	none	6.6
LONG-4.2	108	slight indentation	crack	10.1

^aLONG-2.1 was impacted twice. The second impact was nominally 27 in.-lb.

Because the impact parameters and specimen geometry are different for the LONG and NDT specimens, comparison of the impact test results--such as impact energy vs damage--between the two different graphite/epoxy composites would not be appropriate. In addition, the LONG specimens themselves are not identical. For example, the side of the hat-shaped longeron varied in height along the portion shown in Fig. 8. This variation may have affected the specimens' flexibility and boundary conditions for impact. Thus, the impact response of the composite may vary from specimen to specimen. However, some general observations about the LONG samples can be made.

In the LONG specimens tested, if there was no front surface damage, there was no back surface damage either. Also, from the load and energy vs

time curves, there were obvious points at which the load curve dipped before reaching the maximum load for all longeron impacts. This is in contrast to the impact response of the 48-ply NDT specimens. Whether these dips occurred because of the different material properties, specimen geometries, or impact parameters is not known. For the three impacts where damage was not visible, the load curve dropped relatively smoothly and slowly after the maximum load. This was in contrast to the other three impacts, LONG-2.1, -3.1, and -4.2, where the load dropped suddenly after the maximum load, then oscillated on the way down. Thus, from the load vs time curves, one may differentiate between which impacts produced fiber breakage on the laminate surface and which impacts produced no breakage.

VII. PRE- AND POST-IMPACT NONDESTRUCTIVE EVALUATION

A. X-RAY RADIOGRAPHY

Initially, each NDT and LONG specimen was X-rayed at 30 kV/30 mA for 1 to 2 min, depending on the specimen thickness. The different fiber orientations in the composite laminates were only distinguishable from each other if enough plies at each orientation were present. The extra cloth-weave-type layer, discussed in the laminate orientation section of this report, was visible on the radiographs of LONG-2.1 and LONG-4.2. No damage was detected in the specimens before they were impacted. After impact, the only damage visible on the radiographs was in the form of surface cracks. The X rays were unable to detect internal damage. The X-ray technique merely measures density differences and, therefore, is unable to detect any defect (e.g., a delamination) that does not change the amount of material lying in the X-ray path. However, if the damage extended to the surface, we were able to fill the impacted area with a radiopaque dye. When X-rayed again, the internal damage of the specimen was visible.

The dye was an aqueous 70 wt% solution of a diatrizoate sodium used for gastroenteric radiography. A small amount of Edwal "Kwik-Wet" was added to the solution as a wetting agent. The specimen was placed in a dish inside a chamber, which was evacuated and held at 5 Torr for 30 min. Enough dye was then released into the dish to submerge the specimen. The dye was drawn into delaminations and cracks by capillary action. The vacuum was released after the specimen was submerged. Finally, the specimen was heated sufficiently to remove the water carrier, leaving only a crystallized sodium residue. The process was repeated to increase the residue deposited in the voids. LONG 4.2 was impregnated four times to obtain a good contrast in densities between the dye-enhanced damaged areas and the undamaged areas on the radiographs. The crack widths in the LONG specimens may be smaller than in the NDT specimens; it was more difficult to fill the LONG specimens with the dye than the NDT specimens.

The dye-enhanced specimens were X rayed again at 30 kV/30 mA for 1 to 2 min. On the radiographs, the damaged areas appear white. The size and shape of the impact damaged area were clearly highlighted (see Fig. 11-- print of radiograph). In Figs. 12 and 13, an elliptical damage area is plotted vs energy of impact for the NDT and LONG specimens, respectively. The damage area was calculated using the maximum damage length measured from the radiographs in the 0° and 90° direction. An elliptical damage shape was assumed for the calculation. Greater damage areas were found for specimens with higher energies of impact.

B. ULTRASONICS

The NDT and LONG specimens were ultrasonically C-scanned before and after impact. Through-transmission scanning was performed using 5 MHz transducers. The specimens and the transducers were submerged in water. The damaged specimens were coated with a plastic sealant to prevent water absorption. The resolution of the system was 0.125 in. For consistency with standard practice, the ultrasonic signals were converted to decibels by being referenced to a signal from a known undamaged area on the sample.

The C-scans of the NDT specimens before impact revealed no initial damage. The first scan of the specimen indicated the location of a Teflon insert placed in NDT-6.11 to simulate a delamination (see Fig. 14). Figure 15 illustrates a typical C-scan after impact. A more detailed scan, 0.100 in. resolution, was taken of the damaged area for NDT-6.11 (see Fig. 16). The size and shape of the damage revealed in the C-scan closely resembles the size and shape revealed by X ray (see Fig. 11).

The NDT elliptical damage size measurements from the C-scan data vs impact energy is included in Fig. 12 for comparison with the X-ray data of dye-enhanced specimens. The C-scan damage size followed closely with the X-ray results for all NDT specimens except NDT-4.10. When NDT-4.10 was impact tested, the impactor completely penetrated the specimen and several plies were lifted off the surface of the laminate. While the through-transmission ultrasonic evaluation revealed the internal delamination type

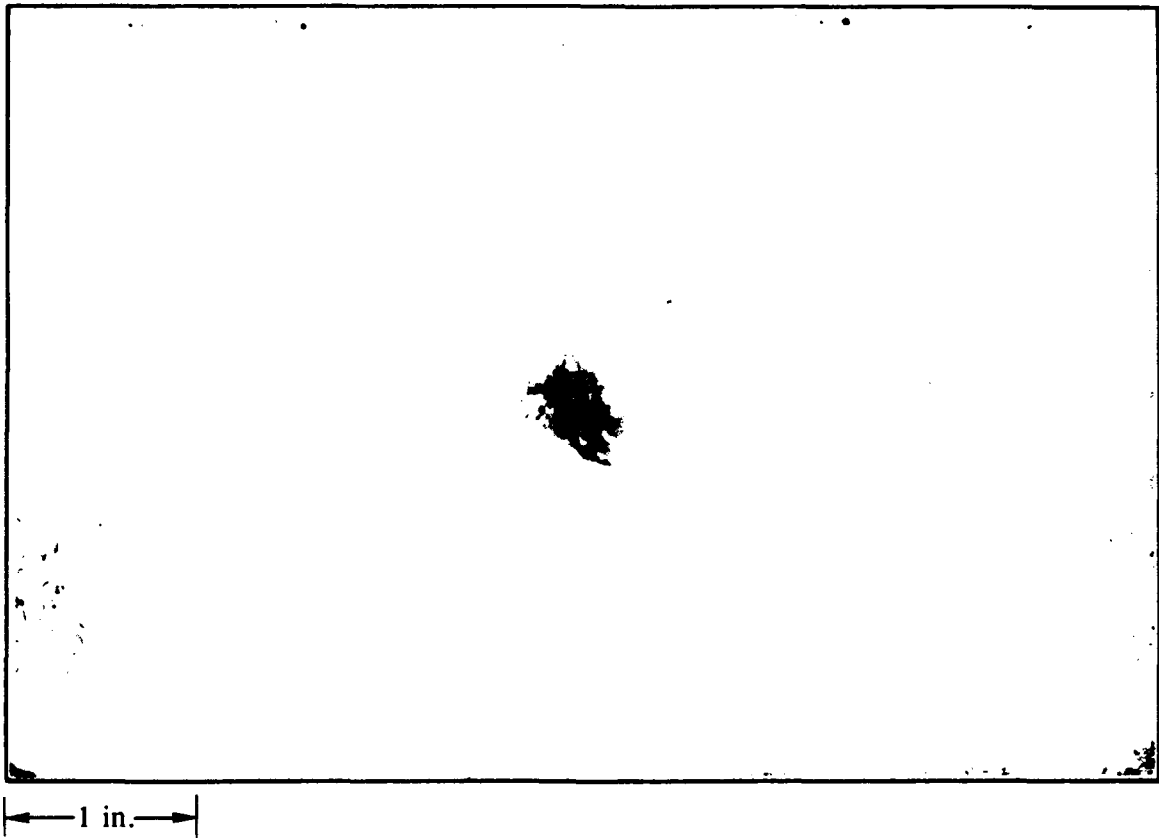


Fig. 11. X ray of Dye-Impregnated NDT-6.11, Highlighting Damaged Area

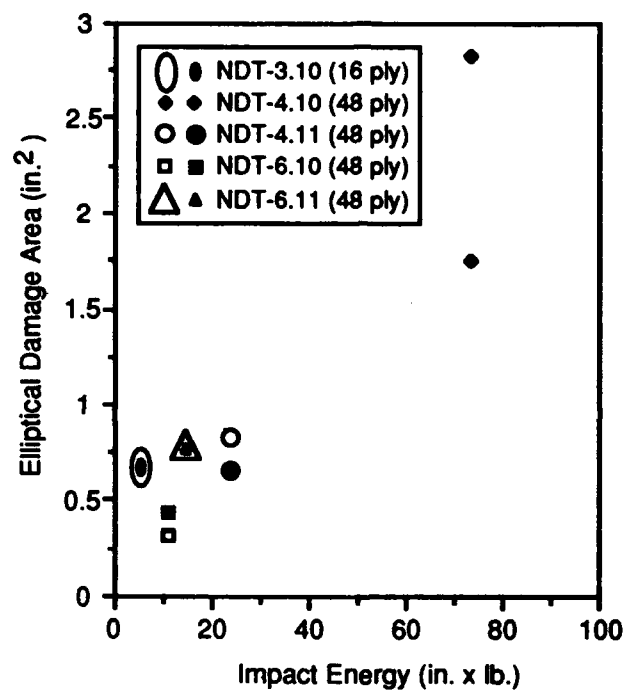


Fig. 12. Elliptical Damage Area Determined from X-ray Radiographs of Dye Enhanced Specimens (open symbols) and C-Scan Data (closed symbols) vs Impact Energy for the NDT Specimens

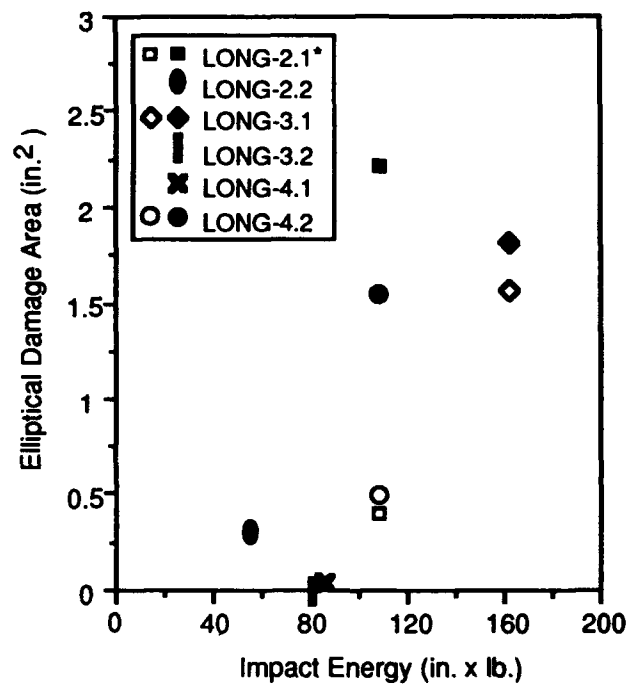


Fig. 13. Elliptical Damage Area Determined from X-ray Radiographs of Dye Enhanced Specimens (open symbols) and C-Scan Data (closed symbols) vs Impact Energy for the LONG Specimens.

*Note: LONG-2.1 was impacted twice. The second impact was nominally 27 in.-lb.

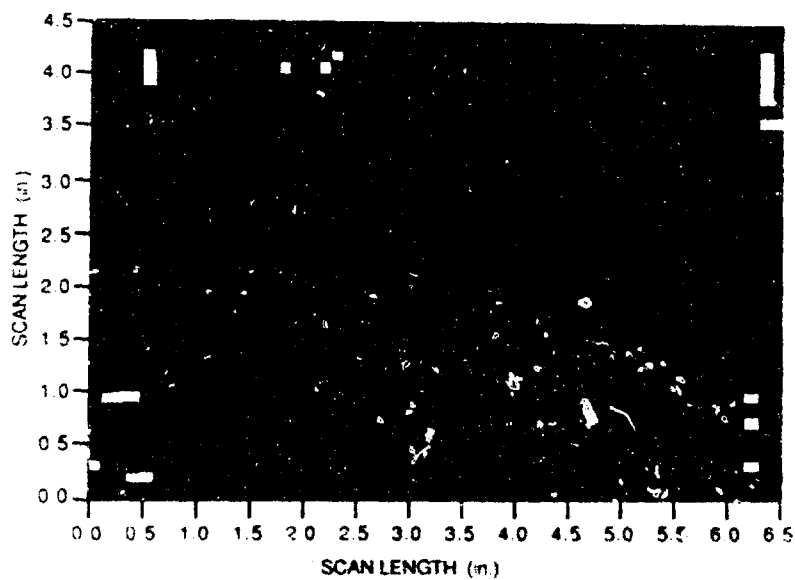


Fig. 14. C-Scan of Specimen NDT-6.11 Prior to Impact.
Note the Teflon insert near the upper left corner.
Specimen holders are evident in each corner.

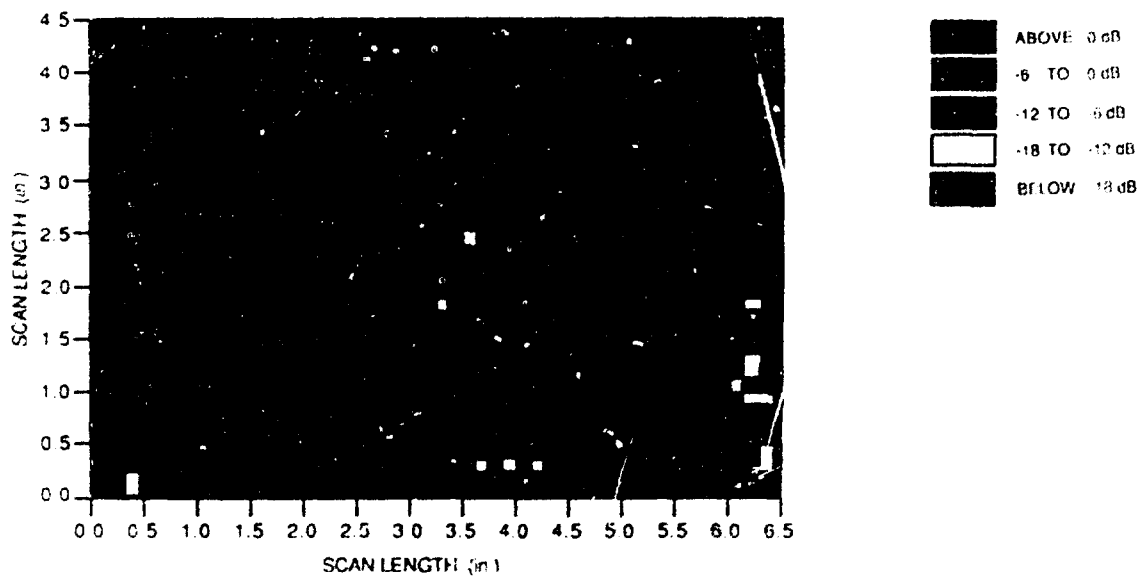


Fig. 15. C-Scan of NDT-6.11 After Being Impacted with 15.6 in.-lb.
Two specimen holders are evident along the bottom of the
specimen. Note the damage area growth near the Teflon
insert.

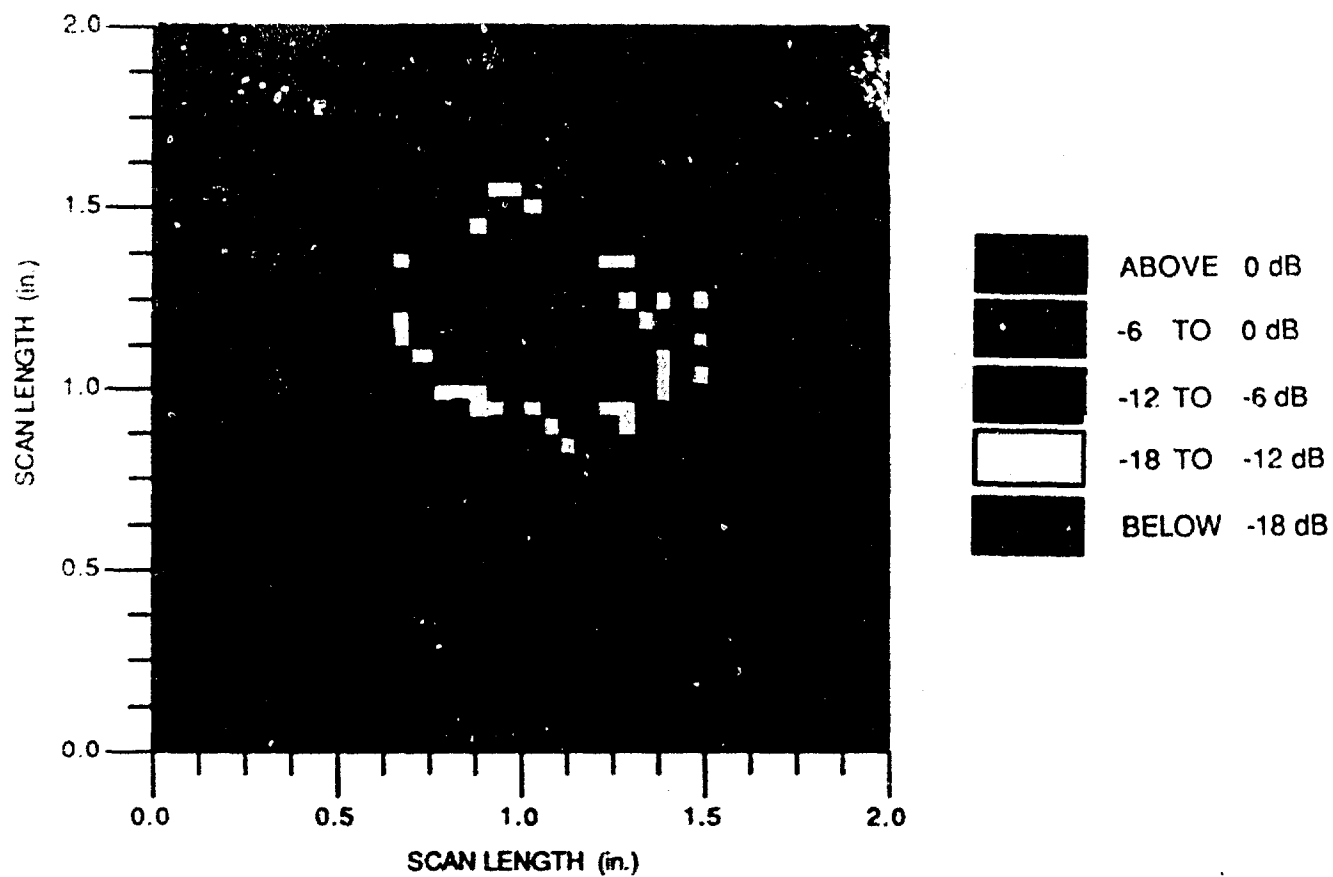


Fig. 16. Detailed Scan of Damaged Area in NDT-6.11. Note the similarity in shape of the damaged area to that revealed with radiopaque dye (see Fig. 10).

damage, this method was not optimized to distinguish the differences between a 48-ply area from an area with a few less plies. However, since X-ray radiography is particularly suited to detecting thickness variations, the extent of surface damage was evident in the radiograph. Therefore, a much higher damage area was associated with NDT-4.10, using the X-ray technique as opposed to the ultrasonic C-scan method.

Ultrasonic C-scan results for the LONG specimens indicated that no significant damage existed before impact testing. Post-impact C-scan damage measurements are plotted vs impact energy in Fig. 13. The most extensive damage occurred in LONG-2.1, but this was the specimen that was inadvertently impacted twice. In comparison with the damage area determined by X-ray radiography, the C-scan results indicate a much larger damage area (see LONG-2.1 and -4.2 in Fig. 13). These differences probably occurred because it was difficult to penetrate these LONG specimens adequately with the radiopaque dye. The crack opening in both these two LONG specimens was tight, and the specimens themselves were much thicker than the NDT specimens. When a LONG specimen was impacted with sufficient energy to produce large cracks, as in LONG-3.1, the damage area detected by the dye-enhanced X-ray method was comparable to that of the ultrasonic method.

Of the three specimens impacted at the lower energies, only LONG-3.2 had no internal damage detected by ultrasonics. LONG-2.2 and -4.1 had small damaged areas, even though these specimens had no visible external damage. Therefore, impact conditions that result in nonvisible damage for these specimens was shown to be possible.

C. THERMAL-ACOUSTIC EMISSION

Acoustic emission (AE) testing is based on the monitoring of stress waves generated by rapid local redistribution of stress. Such stress waves accompany the operation of many damage mechanisms (e.g., crack growth, fiber fracture, plastic deformation) (Ref. 16). Traditionally, AE has been used to detect damage in mechanically loaded composites. Recently, a new

technique, based on the thermal loading of a composite, has been developed. The thermal AE technique is defined as the monitoring of acoustic emission released during the heating and cooling of a damaged composite (Refs. 17, 18).

For our experiment, the NDT specimens were heated with a quartz lamp, as shown in Fig. 17. A Physical Acoustics Corporation (PAC) R151 transducer was attached to the specimen, using a steel clamp. The signal from the transducer was bandpass filtered between 100 to 300 kHz before being sent to a PAC 3000/3004 analyzer. The analyzer also received voltage readings corresponding to temperature from a thermocouple placed alongside the transducer. The specimens were heated from approximately 24 to 56°C at a rate between 1.3 and 1.6°C/sec with the lamp. The specimens were then air cooled to approximately 43°C, or until no AE could be detected. Because of its thickness, the 16-ply specimen, NDT-3.10, was heated at a rate of 2.0°C/sec.

The first run was made on an undamaged specimen cut from NDT-4. The results are graphed in Fig. 18. As expected, no notable AE was detected from the undamaged specimen. When a damaged specimen was tested, AE increased with increased temperature. In their work with carbon-carbon composites, G. F Hawkins et al. attributed the increase in AE signal to the increase in thermal strain caused by the larger thermal gradient (Ref. 16). The results from NDT-4.11 are shown in Fig. 19. The AE data from the four specimens tested indicate an inverse relationship between number of events and impact energy. Also, the amplitude of each event increased with increasing impact energy.

If a specimen was again tested, under the same conditions, little or no AE was detected. These results can be explained by the crack-face friction (CFF) theory. The CFF theory suggests that thermal AE results from a pair of crack faces rubbing against one another. According to N. Sato et al. (Ref. 18), a crack is "anchored" by residual stress. When the damaged composite is thermally loaded, the stress around the crack is released and the crack faces rub against each other, emitting AE. If the residual stress is completely released, there is no AE with successive loading.

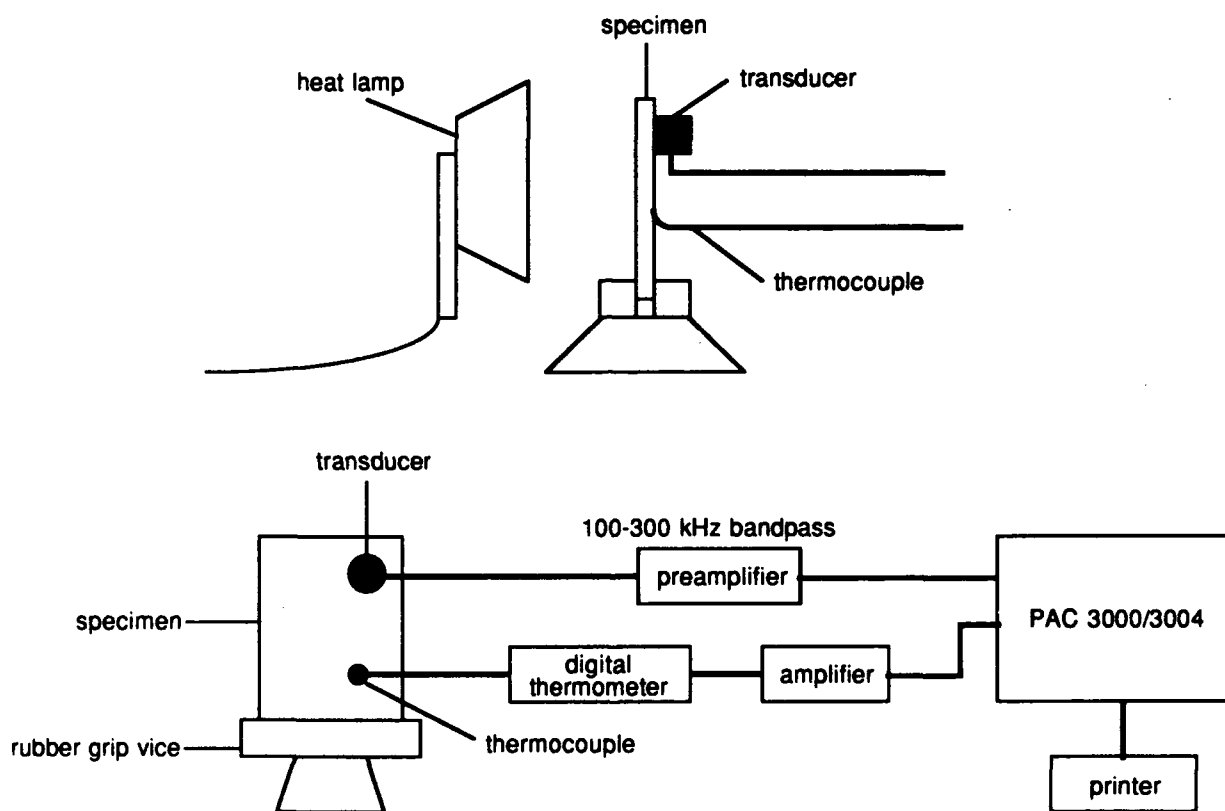


Fig. 17. Thermal-Acoustic Equipment Setup Used to Monitor Acoustic Emission from the NDT Specimens

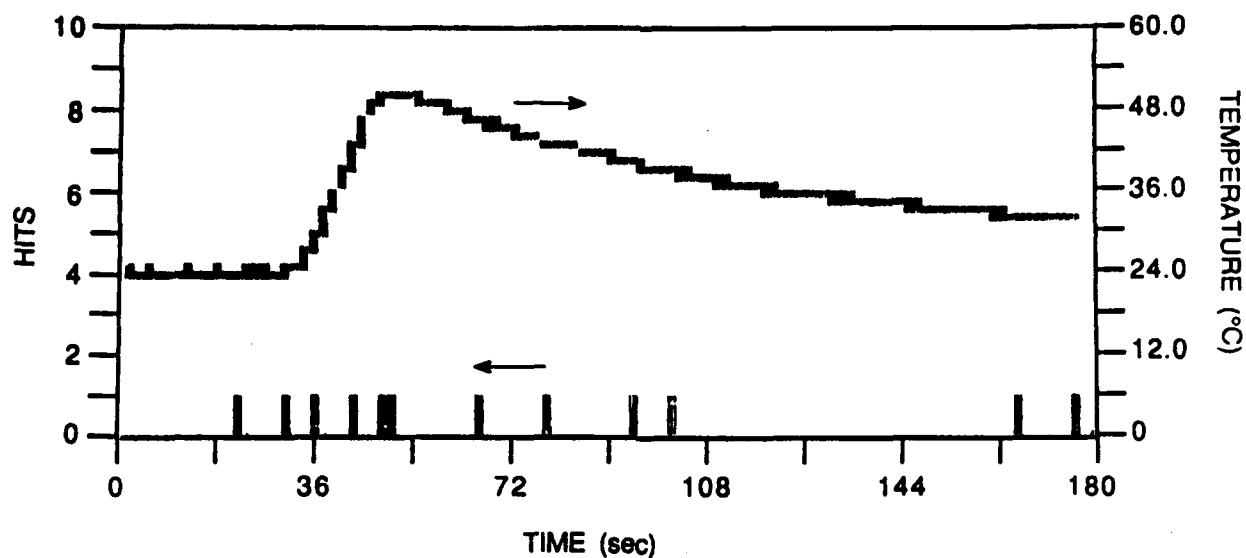


Fig. 18. Acoustic Emission from an Undamaged Specimen

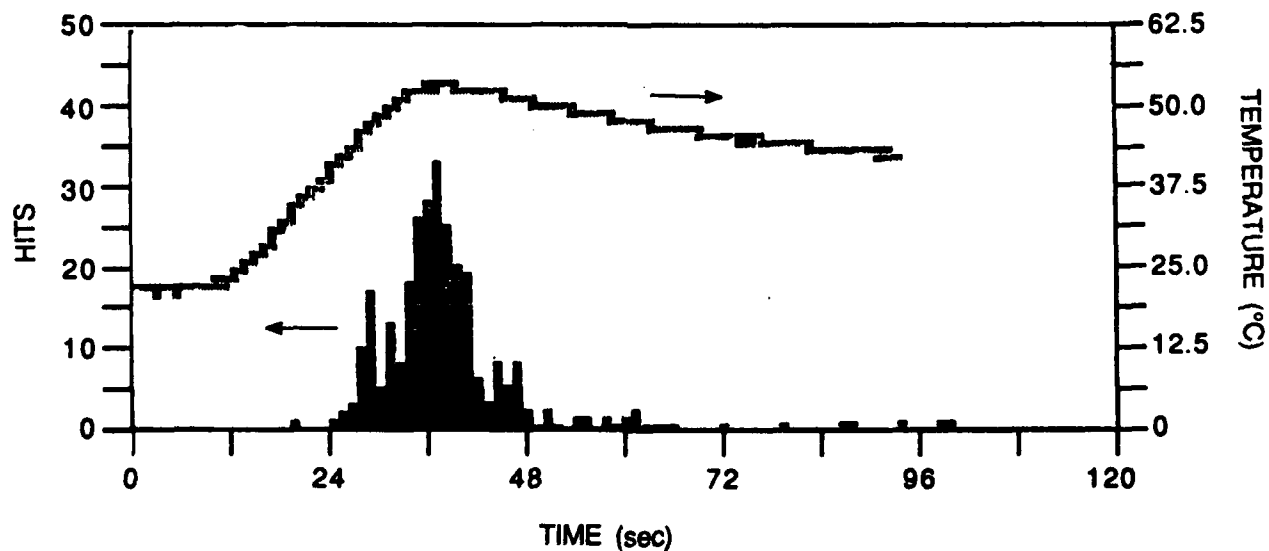


Fig. 19. Acoustic Emission from Specimen NDT-4.11. Total number of hits: 1005. Impact energy of 24.0 in.-lb.

D. THERMOGRAPHY

Each NDT specimen was heated approximately 5°C above ambient temperature with a quartz lamp. The subsequent cooling pattern on the heated surface was recorded using an Inframetrics Model 600 infrared camera. During cooling, the surface above a defect appeared warmer than its surroundings. This occurred because the air gap created by the defect restricted the flow of heat through the surface above the defect area.

The results obtained were poor. Only gross defects close to the heated surface were visible. A "hot spot," indicating a defect, developed, then disappeared, within 1 sec. Thermography is ineffective in detecting defects in materials with high thermal diffusivity, such as graphite/epoxy. Instead of the heat traveling through the material, the high conductivity along the fibers effectively shorts out the effects of any defect. Therefore, the results were comparable to those obtained by visual examination.

E. NDE DISCUSSION

As expected, the damaged area increased with increased impact energy for the NDT specimens. The LONG specimens, because of their nonuniformity, did not yield comparable results. The size and shape of the damaged area can be most effectively determined by impregnating the area with a radio-paque dye and then X-raying the specimen. However, for dye impregnation to be useful, the damaged area must be initially detected by another method, and there must be enough surface damage to allow the dye to penetrate the composite. In addition, the dye must completely penetrate the damaged area. Although dye impregnation is a useful research tool, it would not be practical for inspection of commercial composite structures.

Ultrasonic inspection was used to detect a damaged area and to determine its size. The size of a damaged area found using ultrasonics was in good agreement with the size found using radiopaque dye. When the resolution was adjusted, ultrasonics was effective in obtaining fine details of the internal damage of a specimen. The thermal acoustic inspection of the NDT specimen was useful in determining whether or not the specimen

sustained impact damage. At this time, however, it is difficult to relate the type and amount of composite damage to the emission recorded during heating.

Although visual inspection of the composite surfaces is limited, it did give a reasonable approximation to the relative amount of internal damage. The larger the visible surface damage (cracks), the greater the sustained internal damage (delaminated area). However, in the case of the longeron, no visible damage did not necessarily indicate no internal damage.

Finally, thermography was an inappropriate method to evaluate graphite/epoxy composites because of the high lateral thermal diffusivity of the composites.

VIII. CROSS SECTIONING AND DEPLY ANALYSIS

One impacted specimen, NDT-6.11, was set aside for cross sectioning and deply analysis. NDT-6.11 was cut into three sections through the impact-damaged area using a diamond wire saw. Two of the sections were mounted and polished with one section polished along the 90° normal and the other section along the 0° normal. Figure 20 reveals the polished cross section of the 90° normal section. Recall that the bag side of the laminate was impacted, and therefore ply No. 1 is on the side opposite the impact. Major delaminations could be seen between every 0 and +52° ply sequence except the first one. These delaminations extended about 1/2 in. to each side of the impactor contact point. The size of these delaminations correlates well with the ultrasonic C-scan and X-ray assessment of the damage size. Delaminations were also visible between many +52 and -52° plies and some -52 and 90° plies. Fiber breakage and matrix cracks were found throughout the thickness of the specimen but were confined mainly to just below the point of impact. The polished cross section of the 0° normal section revealed results similar to those found in the 90° normal section.

The third section of NDT-6.11 underwent partial pyrolysis for a ply-by-ply analysis. In the pyrolysis process, the graphite/epoxy composite was heated to 400°C for approximately 12 hours in air, thereby burning off the epoxy resin matrix and leaving the graphite fiber plies intact. Each ply was photographed, then removed one at a time using tweezers, transparent tape, and dental instruments. When two plies of the same fiber orientation were next to each other, only the first ply was photographed, and both plies were removed together. Fiber fracture was easily documented and was shown to exist on nearly all plies between Nos. 1 and 24 and to a smaller extent on many plies between Nos. 25 and 48. Delaminations were not easy to determine. Although the radiopaque dye introduced to the specimen for X-raying left a residue or stain on some of the laminates, the stain was difficult to see. It was not obvious that major delaminations

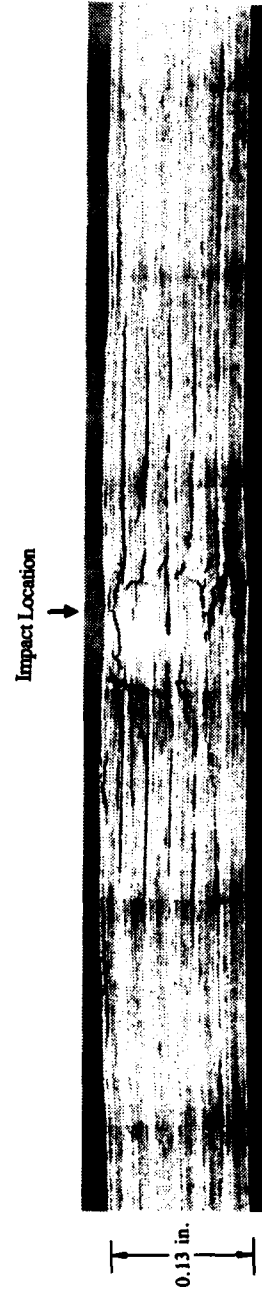


Fig. 20. Photomicrograph of the Cross Section of NDT-6.11 After Impact

occurred between the 0 and 52° plies, as was expected from comparison with the cross-sectioning results. Freeman's technique (Ref. 19) for marking delaminations before deply, using a solution of gold chloride in diethyl ether, should be considered.

IX. POST-IMPACT MECHANICAL TESTING

A. COMPRESSION STRENGTH TESTING

Three of the five impacted NDT specimens were compression tested to failure for residual strength measurements, according to BSS 7260. BSS 7260 is the Boeing Specification Support Standard for testing the compression strength of advanced composite quasi-isotropic laminates with drilled holes or after impact damage. Each specimen had four strain gauges, two on each side, to monitor the distribution of the compression load on the specimen. The specimen and fixture were adjusted and readjusted until the four strain gauges agreed to within 10% of each other during a low load pretest. Because of the thinness of NDT-3.10, it was difficult to make the gauges agree within the prescribed range. Therefore, NDT-3.10 was compression tested with the gauges agreeing to only within 35%. The failure stress results for NDT-4.10, -6.10, and -3.10 are listed in Table 6. NDT-3.10 failed at the edge supports, unlike NDT-4.10 and -6.10, which failed through the central, impact-damaged portion of the plate.

Table 6. Compression Strength Testing Results for the NDT Specimens

Specimen	Laminate Thickness (in.)	Failure Stress (ksi)	Strain Rate (in/sec)	Maximum Strain (in/in)	Approximate Damage Area from C-scan (in. ²)
NDT-4.10	0.14	14.7	0.05	0.31%	1.75
NDT-4.11	0.14	18.9 ^a	0.01	N.A. ^b	0.66
NDT-6.10	0.13	23.6	0.05	0.65%	0.44
NDT-3.10	0.055	9.7 ^c	0.05	0.35%	0.67

^aFailure stress after several load cycles.

^bThis specimen was loaded several times during the acoustic emission monitoring.

^cEarly failure at edge support.

The reduction in compressive strength resulting from the impact damage can be estimated for NDT-4.10 and NDT-6.10 by comparison with the undamaged compression strength results. Unfortunately, the series of mechanical strength tests of undamaged laminates were all done on NDT-1. As reported in Table 3, the compression strength of NDT-1 was 36.2 ksi. Recall that this laminate, although specified by the manufacturer to be a (0/+52/-52/90) type of laminate, actually turned out to have incorrect fiber orientations--namely, 38° fibers were substituted for all except one of the 52° angle plies. Therefore, at this point, no direct correlation can be made between the damaged and undamaged strengths of these P75/934 laminates. A lower compression strength would already be expected for a laminate with 52° fibers as opposed to 38° fibers when undamaged samples were tested for strength in the 0° direction. The relative amount that the strength would be lowered is not easily modelled and would probably best be determined experimentally. Additional undamaged laminates could be obtained with similar fiber orientations to the impacted ones, and the mechanical strength tests could be performed again. Furthermore, a greater number of samples would be necessary to establish a correlation between percent strength reduction with impact energy or damage size. From this study, we can only note that, as expected, the larger the damage area (caused by greater impact energies), the lower the failure stress exhibited by the NDT specimens.

B. ACOUSTIC EMISSION MONITORING DURING COMPRESSION TESTING

NDT-4.10, -6.10, and -3.10 were monitored for AE while being tested for residual compression strength. To further study the AE response of these laminates, NDT-4.11 was subjected to the load history given in Fig. 21. The same compression testing setup was used for NDT-4.11 that was used for the other three specimens. Only the loading rate was changed from 0.05 to 0.01 in. strain/sec for both loading and unloading situations.

AE was monitored by coupling an AET AC175-L (175 kHz) transducer to the specimen with H-R lubricating jelly. The transducer was held in place by a separate fixture from the compression testing fixture. Care was taken

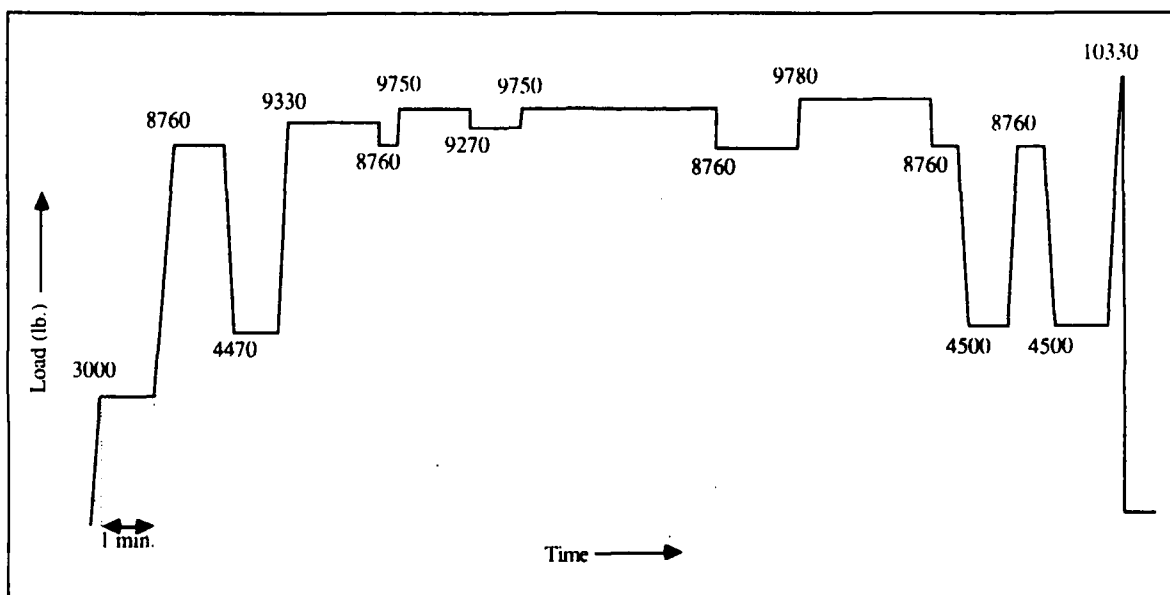


Fig. 21. Load History of NDT-4.11 During Acoustic Emission Monitoring

to avoid exerting a transverse force on the face of the specimen. The acoustic signals detected by the transducers were amplified, measured by an RMS voltmeter, and recorded on a strip chart recorder as a function of time. The load signal was also recorded concurrently on the strip chart.

All three specimens tested for compression strength showed AE activity just before failure as the compressive load was increasing and also after failure when the load had dropped considerably. The AE response of NDT-4.11 can be summarized as follows. The first, small acoustic signal was detected at 8550 lb during the loading up to 8760 lb. There was small-amplitude AE activity commencing at the 8760 and 9330 lb holds, which diminished as the holds continued. AE was detected throughout the entire first 9750 lb hold. During the second 9750 lb hold, AE again started and continued throughout the hold, however, with several much higher amplitude signals. In no instance was there AE during any of the unloading and hold sequences up to this point. All subsequent unloadings and the two 8760 lb holds produced a few, small AE signals. Figure 22 exhibits the AE activity of NDT-4.11 just before, during, and after the second 9750 lb hold. During the 9780 lb hold, moderate AE activity continued. No AE was recorded during the 4500 lb holds. On the final loading, high amplitude AE resumed at 9750 lb and continued past the failure of the specimen and the load drop.

From the AE data, it appears that starting from 9750 lb, significant damage was occurring in the specimen and might have continued to failure if the load had not been reduced. Other researchers have found that, for a carbon-carbon part, AE occurred during load reductions if the part was damaged (Ref. 20). Although the NDT specimens are Gr/Ep composites, as opposed to carbon-carbon, it is interesting to note that for NDT-4.11, no AE occurred during load reductions until after the second 9750 lb hold even though it was already impact damaged.

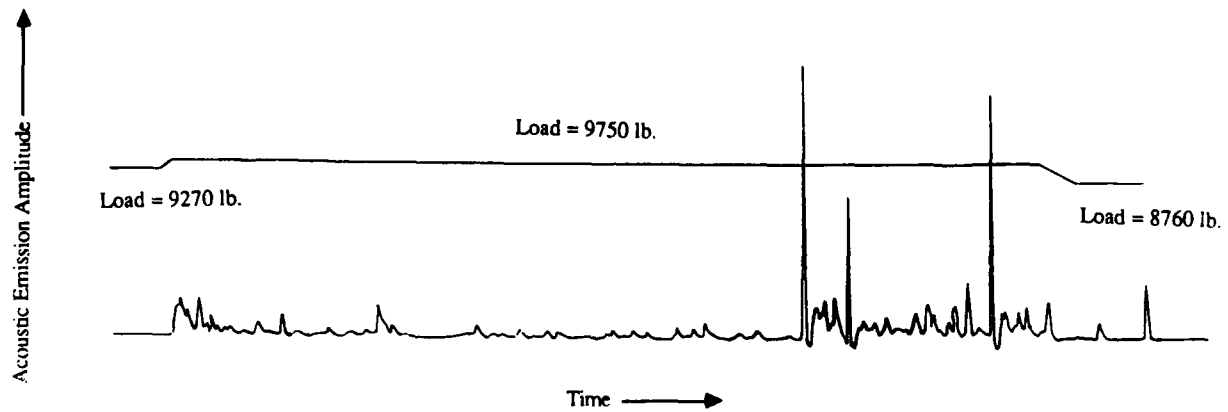


Fig. 22. Acoustic Emission of NDT-4.11 During Compression Loading

X. CONCLUSIONS

This experimental investigation was conducted to study the impact damage response of P75/934 graphite/epoxy laminate plates. Laminate orientation was determined; some thermal, physical, and mechanical properties were measured; impact testing was done with pre- and post-impact NDE; and residual compressive strength was measured. In addition, some work on an HMS/934 graphite/epoxy diagonal longeron was performed.

The low velocity impact testing of the P75/934 laminates revealed that this graphite/epoxy composite system is very susceptible to damage by impact. Impact energies as low as 10 in.-lb. were found to initiate damage in a 48 ply, edge supported, clamped specimen. This measurement corresponds to approximately 6 ft-lb/in. thickness of composite. In comparison, various other graphite/epoxy systems typically undergo damage initiation from 25 to 50 ft-lb/in. thickness of composite. These results indicate the influence of the very high modulus fibers coupled with low toughness, low strength matrix on the impact sensitivity of the composite.

While the P75/934 laminate system was damaged with very small impact energies under the given test parameters, each specimen tested also sustained some surface damage on the side opposite the impact (fine cracks). At higher impact energies, the impacted side of the laminate also had visible surface damage (slight indentations). However, the surface damage could only be visually detected upon careful examination. More specimens need to be tested to establish whether nonvisible surface damage precludes the presence of internal damage. For the HMS/934 longeron specimens, it was shown that internal damage might be present even though no external damage was visible.

The importance of performing laminate microexamination to verify that they conform to the specified fiber orientation and lay-up sequence has been shown. Because the actual laminate orientation for the pre-impact compression strength test specimens was different from the postimpact

laminates tested for residual strength, no direct comparisons could be made in this report. Lower residual compression strengths were observed for specimens impacted with higher energies. However, in order to determine the extent of the strength degradation before impact vs after impact, additional testing, preferably with a larger number of specimens, needs to be performed.

Various NDE methods were applied to detect the impact damage in the composite. Ultrasonic inspection and dye-enhanced X-ray radiography confirmed that the greater the impact energy, the greater the damage area. Because damage caused by impact may not be visible on the front or back composite surface, inspection techniques that would quickly and accurately locate and define internal damage would be useful. Ultrasonic inspection provides excellent NDE of a composite structure; however, frequent, full-scale inspections of large structures would be costly and time consuming. One promising technique addressed in this work was the detection of damage with AE. Large areas of a structure could be heated and then monitored for any AE with an AE transducer. The presence and general location of damage could thus be determined. Once the general location of the damage was established, an ultrasonic inspection of that area would provide the finer details and the extent of the damage. Therefore, further study in understanding the AE response of damaged laminates to heating and cooling would be worthwhile pursuing.

In closing, this investigation has shown that the P75/934 laminate system is sensitive to impact damage. To predict the impact response of an actual large space structure made of this composite material, the geometry and boundary conditions imposed by the structure have to be taken into account. However, when dealing with any P75/934 light hardware, it is important that protection against impacts be considered. Should the structure be impact damaged, techniques to nondestructively detect and evaluate the damage will be required. Corrective action can then be taken to restore the space structure.

REFERENCES

1. J. H. Starnes, M. D., Rhodes, and J. G. Williams, The Effect of Impact Damage and Circular Holes on the Compressive Strength of a Graphite-Epoxy Laminate, NASA-TM-78796, NASA, Washington, DC (1978).
2. S. M. Bishop and G. Dorey, G., "The Effect of Damage on the Tensile and Compressive Performance of Carbon Fibre Laminates," AGARD Conference Proceedings No. 355 (1983).
3. D. Liu, C. T. Sun, and L. E. Malvern, "Structural Degradation of Impacted Graphite/Epoxy Laminates," The Shock and Vibration Bulletin, Part 2 (August 1986), pp. 51-60.
4. M. S. Rosenfeld and L. W. Gause, Compression Fatigue Behavior of Graphite/Epoxy in the Presence of Stress Raisers, ASTM STP 723, ASTM, Philadelphia (1981), pp. 174-196.
5. DOD/NASA Advanced Composite Design Guide, AFWAL/FIBCA, Wright Patterson AFB, Ohio (July 1983).
6. C. L. Johnson and J. B. Cushman, Stress Concentration Design Data for P75S/934 Composite, (to be published).
7. Advanced Composite Compression Tests, Boeing Specification Support Standard BSS 7260 (1983).
8. R. M. Aoki, "Behavior of Idealized Discontinuities and Impact Damages in CFRP Under Fatigue Loading," AGARD Conference Proceedings, No. 355 (1983).
9. R. A. Garrett, "Effect of Manufacturing Defects and Service-Induced Damage on the Strength of Aircraft Composite Structures," 17th National SAMPE Technical Conference (October 1985).
10. B. Soulezelle, "Low Velocity Impacts on Carbon Resin Composites Influence of Experimental Conditions," Looking Ahead for Materials and Processes, J. de Bossu, et al., eds., Elsevier Science Publishers, Amsterdam (1987).
11. K. K. Stellbrink and R. M. Aoki, "Effect of Defect on the Behaviour of Composites," Progress in Science and Engineering of Composites, Y. Hayashi et al., eds., ICCM-IV, Tokyo (1982).
12. R. J. Palmer, Investigation of the Effect of Resin Material on Impact Damage to Graphite/Epoxy Composites, NASA CR-165677 (1981).

13. A. A. Baker, R. Jones, and R. J. Callinan, "Damage Tolerance of Graphite/Epoxy Composites," Composite Structures (1985), pp. 15-44.
14. T. A. Sollars, Shuttle/Centaur G-Prime Composite Adapters Damage Tolerance/Repair Test Program, AIAA (1987), pp. 362-375.
15. L. W. Gause and L. J. Buckley, Impact Characterization of New Composite Materials, ASTM STP 936, S. L. Kessler et al., eds., ASTM, Philadelphia (1987) pp. 248-261.
16. M. Hamstead, "A Review: Acoustic Emission, a Tool for Composite-Materials Studies," Experimental Mechanics, Vol. 1 (March 1986), pp. 7-13.
17. G. F. Hawkins, M. Buechler, and R. A. Meyers, Acoustic Emission Testing and Microstructure Evaluation of Carbon-Carbon Composites, TR-85-062, AFAL, Edwards Air Force Base, California (August 1985).
18. N. Sato, T. Karauchi, and O. Kamigaito, "Thermo-Acoustic Emission From Damaged Composite," 31st International SAMPE Symposium and Exhibition Proceedings (April 1986), pp. 342-351.
19. S. M. Freeman, "Characterization of Lamina and Interlaminar Damage in Graphite/Epoxy Composites by the Deply Technique," Composite Materials: Testing and Design (6th Conference), ASTM STP 787, I. M. Daniel, ed., ASTM, Philadelphia (1982), pp. 50-62.
20. G. F. Hawkins, M. Buechler, and R. A. Meyer, "Acoustic Emissions During Stress Reduction," in Review of Progress in Quantitative NDE, Vol. 4B, D. O. Thompson and D. E. Chimenti, eds., Plenum Publishing Corporation (1985).

LABORATORY OPERATIONS

The Aerospace Corporation functions as an "architect-engineer" for national security projects, specializing in advanced military space systems. Providing research support, the corporation's Laboratory Operations conducts experimental and theoretical investigations that focus on the application of scientific and technical advances to such systems. Vital to the success of these investigations is the technical staff's wide-ranging expertise and its ability to stay current with new developments. This expertise is enhanced by a research program aimed at dealing with the many problems associated with rapidly evolving space systems. Contributing their capabilities to the research effort are these individual laboratories:

Aerophysics Laboratory: Launch vehicle and reentry fluid mechanics, heat transfer and flight dynamics; chemical and electric propulsion, propellant chemistry, chemical dynamics, environmental chemistry, trace detection; spacecraft structural mechanics, contamination, thermal and structural control; high temperature thermomechanics, gas kinetics and radiation; cw and pulsed chemical and excimer laser development, including chemical kinetics, spectroscopy, optical resonators, beam control, atmospheric propagation, laser effects and countermeasures.

Chemistry and Physics Laboratory: Atmospheric chemical reactions, atmospheric optics, light scattering, state-specific chemical reactions and radiative signatures of missile plumes, sensor out-of-field-of-view rejection, applied laser spectroscopy, laser chemistry, laser optoelectronics, solar cell physics, battery electrochemistry, space vacuum and radiation effects on materials, lubrication and surface phenomena, thermionic emission, photosensitive materials and detectors, atomic frequency standards, and environmental chemistry.

Electronics Research Laboratory: Microelectronics, solid-state device physics, compound semiconductors, radiation hardening; electro-optics, quantum electronics, solid-state lasers, optical propagation and communications; microwave semiconductor devices, microwave/millimeter wave measurements, diagnostics and radiometry, microwave/millimeter wave thermionic devices; atomic time and frequency standards; antennas, rf systems, electromagnetic propagation phenomena, space communication systems.

Materials Sciences Laboratory: Development of new materials: metals, alloys, ceramics, polymers and their composites, and new forms of carbon; nondestructive evaluation, component failure analysis and reliability; fracture mechanics and stress corrosion; analysis and evaluation of materials at cryogenic and elevated temperatures as well as in space and enemy-induced environments.

Space Sciences Laboratory: Magnetospheric, auroral and cosmic ray physics, wave-particle interactions, magnetospheric plasma waves; atmospheric and ionospheric physics, density and composition of the upper atmosphere, remote sensing using atmospheric radiation; solar physics, infrared astronomy, infrared signature analysis; effects of solar activity, magnetic storms and nuclear explosions on the earth's atmosphere, ionosphere and magnetosphere; effects of electromagnetic and particulate radiations on space systems; space instrumentation.